European Journal of Medicinal Chemistry 285 (2025) 117214

Contents lists available at ScienceDirect

European Journal of Medicinal Chemistry

journal homepage: www.elsevier.com/locate/ejmech

Research paper

Multicationic ruthenium phthalocyanines as photosensitizers for photodynamic inactivation of multiresistant microbes

Ana Belén Domínguez [a], Daniel Ziental [b], Jolanta Dlugaszewska [c], Lukasz Sobotta [b,**], Tomás Torres [a,d,e,***], M. Salomé Rodríguez-Morgade [a,d,*]

[a] Departamento de Química Orgánica, Universidad Autónoma de Madrid, Cantoblanco, 28049, Madrid, Spain
[b] Chair and Department of Inorganic and Analytical Chemistry, Poznan University of Medical Sciences, Rokietnicka 3, 60-806, Poznan, Poland
[c] Chair and Department of Genetics and Pharmaceutical Microbiology, Poznan University of Medical Sciences, Rokietnicka 3, 60-806, Poznan, Poland
[d] Institute for Advanced Research in Chemical Sciences (IAdChem), Universidad Autónoma de Madrid, Cantoblanco, 28049, Madrid, Spain
[e] IMDEA-Nanociencia, c/Faraday 9, Cantoblanco, 28049, Madrid, Spain

ARTICLE INFO

Keywords:
Phthalocyanines
Ruthenium
Singlet oxygen
PDI
aPDT
MRSA
ESBL+
PACT

ABSTRACT

Four photosensitizers **PS1a-PS4a** consisting in multicationic ruthenium(II) phthalocyanines (RuPcs) have been evaluated in photodynamic inactivation (PDI) of multiresistant microorganisms. The RuPcs, bearing from 4 to 12 terminal ammonium salts, have been designed to target the microorganisms cytoplasmic cell membrane and display high singlet oxygen quantum yields. In addition, **PS3a** and **PS4a** were conceived to exhibit multi-target localization by endowing them with amphiphilic character, using two different structural approaches. Under low light regimes, the two hydrophilic **PS1a** and **PS2a**, as well as the amphiphilic **PS3a** show much stronger response against Gram-positive *MRSA* than that observed for the typical phthalocyanines designed for PDI, namely zinc(II) and palladium(II) complexes, as well as free-base Pcs. Besides, **PS1a**, **PS2a** and **PS3a** show remarkably high activity against the Gram-negative *E. coli*, although weak fungicidal character against fluconazole-resistant *C. albicans*. Contrasting, the structurally different, amphiphilic **PS4a** shows only slight activity for Gram-positive bacteria, despite its ability to cross cell membrane and reach internal organelles. Still, **PS4a** shows a positive synergistic effect against *MRSA* when combined with doxycycline, exhibiting an increased activity from about 1.5 to about 4.9 log reduction under the light dose of 30 J/cm^2 and the 0.125 mg/L subinhibitory dose of doxycycline.

1. Introduction

The rise of antibiotic resistance has led to the emergence of photodynamic inactivation (PDI), also known as antimicrobial PDT (aPDT) or photodynamic antimicrobial chemotherapy (PACT), as a promising alternative to traditional antibiotic treatments. PDI utilizes a non-toxic, photosensitive drug called photosensitizer (PS), specific-wavelength light, and molecular oxygen, to produce reactive oxygen species (ROS), such as singlet oxygen ($^1O_2$), which effectively damages essential structures in microorganisms, neutralizing their viability. This approach has shown effectiveness across a wide range of pathogens, including bacteria, fungi, viruses, and parasites [1,2]. PDI involves the absorption of photons by the PS, leading to the promotion of electrons to a singlet excited state (S_1) and subsequent transition to a long-lived triplet excited state (T_1) through intersystem crossing (ISC) [3,4]. T_1 can participate in two types of reactions: Type-I reactions involve hydrogen or electron transfer, generating reactive oxygen species (ROS), while Type-II reactions transfer energy to molecular oxygen to produce highly reactive $^1O_2$, capable of causing oxidative stress and damaging cellular structures [5–7]. Lately, the possibility of the type-III reaction occurrence, which involves direct interaction between excited sensitizer and target molecule, has been reported by Hamblin and Abrahamse [8].

The multi-target mechanism of photodynamic inactivation (PDI) presents a significant advantage over traditional antimicrobials by

* Corresponding author. Departamento de Química Orgánica, Universidad Autónoma de Madrid, Cantoblanco, 28049, Madrid, Spain.
** Corresponding author. Chair and Department of Inorganic and Analytical Chemistry, Poznan University of Medical Sciences, Rokietnicka 3, 60-806, Poznan, Poland.
*** Corresponding author. Departamento de Química Orgánica, Universidad Autónoma de Madrid, Cantoblanco, 28049, Madrid, Spain.
E-mail addresses: lsobotta@ump.edu.pl (L. Sobotta), tomas.torres@uam.es (T. Torres), salome.rodriguez@uam.es (M.S. Rodríguez-Morgade).

https://doi.org/10.1016/j.ejmech.2024.117214
Received 9 November 2024; Received in revised form 19 December 2024; Accepted 25 December 2024
Available online 27 December 2024
0223-5234/© 2025 The Authors. Published by Elsevier Masson SAS. This is an open access article under the CC BY-NC license (http://creativecommons.org/licenses/by-nc/4.0/).

making it highly unlikely for microorganisms to develop resistance. Unlike conventional treatments that often target a single pathway, PDI operates uniquely. In PDI, the cytoplasmic membrane, which contains proteins and enzymes susceptible to the effects of the ROS and $^1O_2$ generated during the process, is the primary target for microbial inactivation [9,10]. This leads to a substantial reduction in membrane transport capacity, hindering essential substrate uptake needed for microorganism metabolism. Additionally, the PS can penetrate into the inner cellular regions, extending the reach of photooxidative reactions beyond the membrane [11].

PS delivery methods such as topical application, instillation, injection, or aerosol administration ensure localized distribution, minimizing the risk of harming healthy tissues—a crucial consideration in infection treatment [12]. Furthermore, the potential of PDI lies in designing PSs that selectively bind to microbial cells while sparing host mammalian cells from harm. By exploiting the greater negative charge displayed by certain microbial cells compared to mammalian cells, cationic functionalities can be introduced to PS molecules to achieve selectivity. Thus, cationic PSs, including phenothiazines, porphyrins, and phthalocyanines, have emerged as highly effective options for clinical PDI, making them preferred choices for combating infections [13–22].

To effectively evaluate PSs for PDI, several crucial factors and properties must be considered [23–25]: (i) the PS should be a well-defined, single, and pure substance with a stable composition; (ii) it should exhibit minimal dark toxicity; (iii) the PS should absorb light efficiently and be activated upon exposure to appropriate wavelengths, typically falling within the 600–800 nm range; (iv) it should have a strong ability to generate singlet oxygen in high quantum yield and (v) the PS should demonstrate substantial light-dependent cytotoxicity, effectively inducing cellular damage upon activation.

Phthalocyanines (Pcs) are increasingly utilized as PSs for $^1O_2$ generation in PDT and PDI applications due to a number of properties that make them advantageous [26–33]: (i) Pcs exhibit efficient light absorption in the red region of the electromagnetic spectrum, typically ranging from 650 to 700 nm. This absorption range can be extended further into the NIR region by modifying the Pc structure [34]. (ii) Certain Pc derivatives excel as PSs due to their high triplet quantum yield (Φ_t) and extended lifetime (τ_t), resulting in high singlet oxygen generation with notable quantum yield (Φ_Δ). Additionally, the ability of Pcs to form various metal complexes enhances their singlet oxygen production potential [35,36]. (iii) Pcs offer significant flexibility for customization through chemical modifications, allowing fine-tuning of properties like hydrophilicity/lipophilicity, and targeting specificity to meet PDI requirements [37].

The low solubility of Pcs in physiological environments that can hinder their direct administration, as well as their high tendency to aggregate in solution constitute their main drawbacks. In the context of PDI, advantageous cationic functional groups that can be covalently attached to the Pc macrocycle impart water solubility and prevent PS aggregation in cellular media [27,35]. The latter is crucial, as aggregation can lead to reduced singlet oxygen quantum yields [38]. In this respect, cationic Pc derivatives can be synthesized through quaternization of nitrogen atoms present in their substituents [30]. Besides, Pc aggregation depends on various factors such as size, substitution pattern, solvent nature, temperature, and concentration. By introducing bulky and/or axial substituents, aggregation can be minimized or eliminated, thereby enhancing Pc performance as PSs for PDI [39–41].

There are several Ru(II) complexes that have shown effectivity in PDI [42,43]. However, studies on the evaluation of ruthenium(II) phthalocyanines (RuPcs) as PSs for antimicrobial activity are very scarce, despite the potential advantages that these derivatives offer with respect to other Pc complexes [44,45]. In principle, the heavy Ru atom stabilizes triplet excited states and induces high Φ_Δ [46–48]. Furthermore, RuPcs form stable and rigid structures through metal coordination with σ-donor, π-acceptor axial pyridine ligands, this precluding aggregation and leading to high triplet excited state yields and efficient singlet oxygen generation [46,49,50]. Additionally, axial substituents can be designed to add some desired properties, such as hydrophilicity or specific targeting. Indeed, we have already proved the high efficiency of RuPcs bearing hydrophilic and/or targeting motifs at the axial positions for bladder cancer PDT [49,51–53]. In this report, we have prepared four cationic RuPcs **PS1a-PS4a** (Fig. 1) bearing different number − i.e. from 4 to 12 − of terminal ammonium salts decorating their axial substituents. These PSs were prepared by quaternization of the neutral amino functions of the corresponding RuPcs **PS1**-**PS4**. To enhance their penetration through the membrane, two of the PSs, namely, **PS3a** and **PS4a**, have been designed with amphiphilic character, by combining the hexacationic axial substitution with lipophilic axial (**PS3a**) or peripheral (**PS4a**) functionalization. The chemical and photochemical properties of **PS1a-PS4a**, namely their solubility, their ability to generate $^1O_2$ and their lipophilicity, have been determined. Screening for Gram-positive methicillin-resistant *Staphylococcus aureus* (MRSA) and Gram-negative *E. coli* producing extended spectrum of beta-lactamases (ESBL+), as well as for fluconazole resistant *Candida albicans*, are also included.

2. Results and discussion

2.1. Synthesis

The preparation of the PSs starts with the synthesis of the pyridine derivatives **L1**, **L2** and **L3** (Scheme 1) containing either hydrophilic substituents with terminal amine functions for their quaternization in further steps, or lipophilic rests such as long alkyl chains. Both types of ligands were generated through chemical manipulation of pyridine-3,5-dicarboxylic acid (Scheme 1). The synthesis of pyridine ligand **L1**, functionalized with two polyether (PEG) chains bearing terminal amino groups, was accomplished by modifying our previously reported procedure [51]. The two carboxylic groups of pyridine-3,5-dicarboxylic acid were activated through conversion into N-succinimidyl intermediate **1** *via* reaction with N-hydroxysuccinimide in the presence of trifluoroacetic anhydride and pyridine, following a reported procedure [54]. This enabled the esterification reaction with the commercially available 2-[2-(dimethylamino)ethoxy]ethanol, ultimately affording **L1**.

The preparation of **L2** is shown in Scheme 1. The alkylation reaction of gallic acid methyl ester with 2-dimethylaminoethyl chloride hydrochloride resulted in the ester **2**, which was reduced with $LiAlH_4$ to afford alcohol **3**. The esterification reaction between **1** and **3** afforded the pyridyl ligand **L2**.

The ^{1}H NMR spectrum of **L1** (Fig. S1) displays the signals corresponding to the pyridine ring at 9.37 and 8.87 ppm, appearing as a doublet and a triplet, respectively (J = 2.1 Hz). The –CH_2- protons appear as four triplets at 4.54, 3.81, 3.62 and 2.52 ppm, while the singlet at 2.26 ppm corresponds to the –NCH_3 proton signals. The ^{1}H NMR spectrum of **L2** (Fig. S3) shows a doublet (J = 2.2 Hz) and a triplet (J = 2.2 Hz) at 9.37 and 8.89 ppm, respectively, corresponding to the two magnetically different pyridine protons. The singlets at 6.67 and 5.30 ppm are assigned to the H-2′,6′ benzene and benzylic protons, respectively, while the –OCH_2– group appears as a multiplet at 4.09 ppm, and the –NCH_2– group is seen as a multiplet at 2.74 ppm. Finally, the –N$(CH_3)_2$ methyl protons are observed at 2.36 ppm.

The synthetic pathway for the lipophilic ligand **L3** containing six dodecanyloxy chains is depicted in Scheme 1. The alkylation reaction of gallic acid methyl ester with dodecyl 4-methylbenzene sulphonate (**4**) gave the ester **5**, which was reduced using $LiAlH_4$ leading to alcohol **6**. Next, **L3** was obtained *via* esterification reaction between alcohol **6** and pyridine-3,5-dicarboxylic acid in the presence of DIPEA and COMU as carboxyl activating agent. The ^{1}H NMR spectrum of **L3** (Fig. S7) exhibits a doublet and a triplet, respectively (J = 2.1 Hz), at 9.38 and 8.90 ppm, which are attributed to the pyridine ring. The singlets at 6.63 and 5.30 ppm correspond to the H-2′,6′ benzene and benzylic protons, respectively. The –OCH_2- group appears as a multiplet ranging from 4.00 to 3.93 ppm. Additionally, multiplets at 1.84–1.60 and 1.49–1.44 ppm

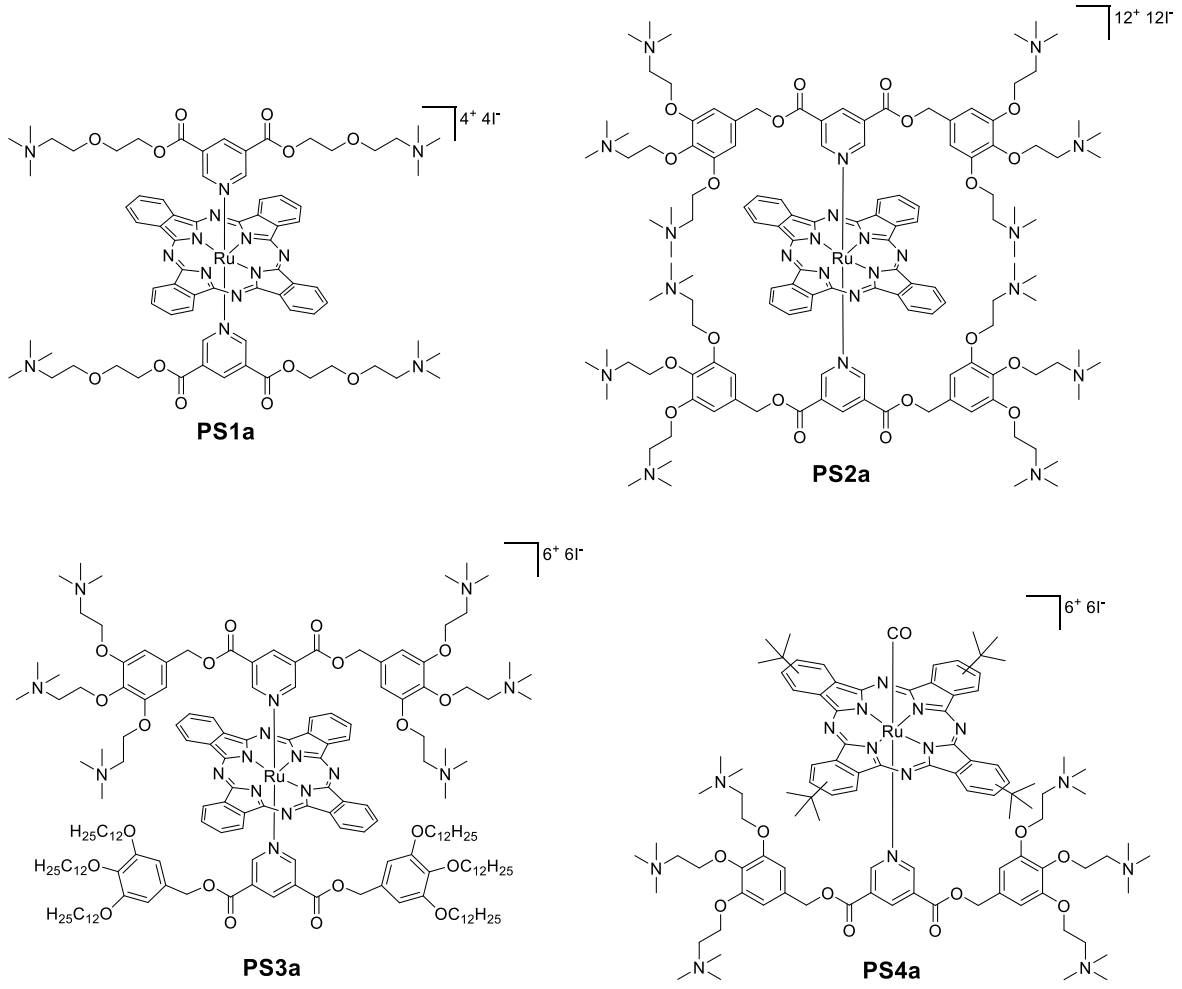

Fig. 1. Chemical structures of **PS1a**, **PS2a**, **PS3a** and **PS4a**.

correspond to the subsequent two CH_2 groups nearest to the aromatic ring (H-3''; H-4''). The remaining $-CH_2-$ groups of the aliphatic chains collectively appeared at 1.26 ppm as a singlet. Finally, the multiplet at 0.90–0.85 ppm corresponds to the terminal $-CH_3$ protons.

With respect to the synthesis of the RuPcs, two different scaffolds are used in this work, namely, peripherally unsubstituted RuPcs and tetra-*tert*-butyl substituted RuPc. This choice relies in the high Φ_Δ observed for these substitution patterns [35,49,51–53]. The peripherally unsubstituted RuPcs were endowed with two pyridyl ligands at the axial positions by replacing the relatively labile nitrile ligands in a preformed bis-benzonitrile RuPc intermediate **Ru(PhCN)$_2$Pc** [51] (Scheme 2, Table 1), by strongly coordinated pyridyl-based ligands [55,56]. By using this sequence, two hydrophilic (**PS1** and **PS2**) and one amphiphilic PSs (**PS3**) were prepared. Hydrophilic RuPcs **PS1** and **PS2** containing four and twelve terminal amino groups, respectively, distributed in two identical axial ligands, were achieved by treating **Ru(PhCN)$_2$Pc** with excess of **L1** or **L2**, respectively. The amphiphilic, asymmetric **PS3** (Scheme 2, Table 1) was obtained from the same **Ru(PhCN)$_2$Pc** intermediate by using an equimolecular mixture of the hydrophilic **L2** and the hydrophobic **L3** pyridine derivatives, resulting in a mixture of three different phthalocyanines, namely, two axially symmetrical RuPcs, and the desired axially unsymmetrical complex. **PS3** was separated from the other products and from the excess of ligands by size exclusion chromatography in Biobeads using dichloromethane as the eluent. The specific quantities of reactants, reaction temperatures, and solvents used for each reaction are detailed in Table 1.

Fig. 2, S11, S15 and S19 illustrate the comparative ^{1}H NMR spectra in $CDCl_3$ of **PS1-PS3** related to **Ru(PhCN)$_2$Pc** and **L1-L3** ligands. In **PS1** (Fig. S11) both α and β protons of the phthalocyanine core are shielded from 9.30 ppm and 7.96 ppm to 9.21 ppm and 7.92 ppm, respectively, upon replacement of the nitrile by the pyridyl ligand, hence enabling monitoring the progress of the reaction by ^{1}H NMR. As for all RuPcs described here, the axial ligands are influenced by the diatropic ring current of the phthalocyanine, falling within the shielding cone. Consequently, all signals corresponding to the pyridyl ligands shift to higher fields upon coordination to RuPc. The anisotropic effect becomes more pronounced as the proton approaches the Pc ring. For instance, upon coordination of **L1** to RuPc, the H-2,6 pyridyl protons exhibited a high-field shift of 6.26 ppm, while the H-4 proton appeared shifted by 1.68 ppm. Similarly, all PEG protons experienced shielding upon coordination to RuPc, with the signal corresponding to $-COOCH_2-$ showing an upfield shift of 0.66 ppm, while the resonances of $-NCH_2-$ and $-N(CH_3)_2$, are further apart, shifted by 0.13 and 0.08 ppm, respectively. **PS2** shows similar chemical shifts of the RuPc ring and the coordinated **L2** (Fig. S15). In particular, resonances corresponding to the RuPc ring appear at 9.09 and 7.87 ppm, while the H-2,6 and H-4 pyridyl protons are detected at 3.07 and 7.14 ppm, respectively. Besides, the benzylic proton is observed as a singlet at 6.23 ppm, 0.44 ppm upfield shifted with respect to the free ligand. With respect to **PS3**, upon coordination to the RuPc, the signals corresponding to **L2** and **L3** experience comparable effects to those of the corresponding symmetric RuPcs, verifying the desymmetrization of the molecule through the splitting of the resonances, which appears particularly evident for the axial substituents (see Fig. 2 and S19). Thus, the H-2,6 and H-4 protons of the two pyridyl

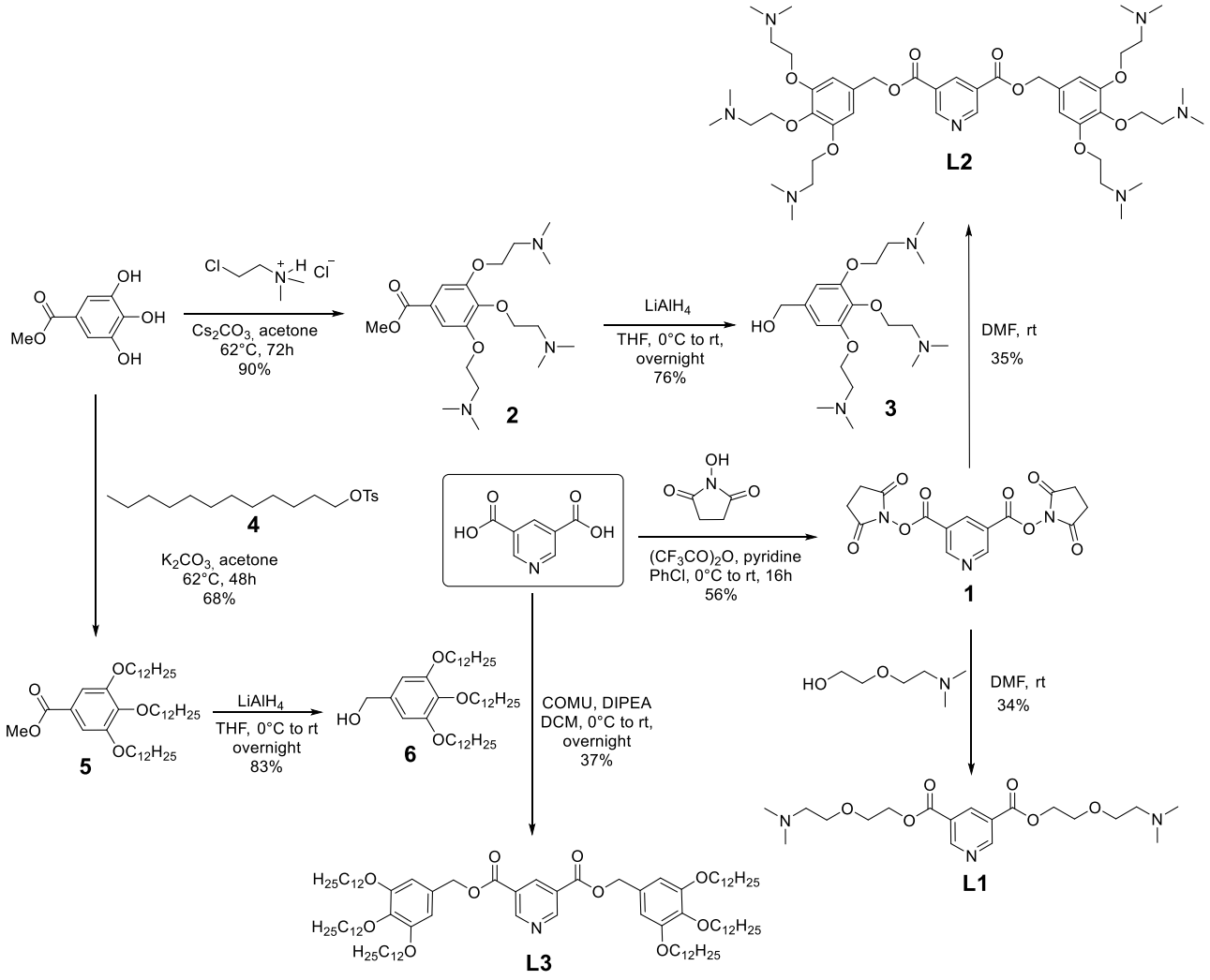

Scheme 1. Synthesis of **L1**, **L2** and **L3**.

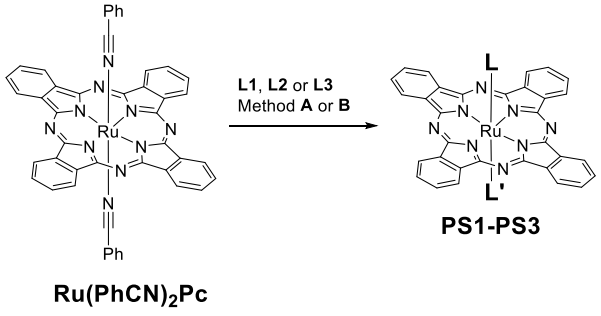

Scheme 2. Preparation of **PS1-3**.

Table 1
Reaction conditions for the preparation of **PS1-3**.

Product	$Ru(PhCN)_2Pc$ (mol)	L1 (mol)	L2 (mol)	L3 (mol)	Method[a]	Yield[b]
PS1	1	2.25	–	–	A	79
PS2	1	–	2.25	–	A	49
PS3	1	–	1.10	1.10	B	8

[a] A: Toluene, 60 °C. B: $CHCl_3$, rt.
[b] Isolated product.

ligands are distinguished as two sets of resonances at 3.07 and 3.06 ppm for the former, and 7.16 and 7.13 for the latter. In addition, two clear singlets are detected for the two nonequivalent axial benzylic protons at 6.22 and 6.20 ppm.

To enhance water solubility, preclude aggregation [35], and make the compounds more active towards pathogen cell membranes, ammonium salts **PS1a-PS3a** were prepared by amine quaternization from the respective **PS1-PS3** by treatment with MeI in DMF (Scheme S1). Complete methylation was confirmed by ^{1}H NMR in DMSO-d_6.

The preparation of the other amphiphilic RuPc **PS4a** was performed using a one-pot synthesis in which the tetra-*tert*-butyl-ruthenium phthalocyanine scaffold **Ru(CO)Pc** (Scheme 3), coordinating a carbonyl ligand at one of the Ru(II) axial coordination sites, was treated with **L2**, following reported procedures [48,50,56]. The progress of the reaction was monitored until completion using ^{1}H NMR spectroscopy and once concluded, **PS4** was *in situ* treated with MeI in DMF (Scheme S1), yielding 19 % of the hexacationic compound calculated over the two steps.

The ^{1}H NMR spectra of **PS1a-PS4a** are expected to show deshielded $(CH_3)_3N^+$– protons compared to the corresponding amino substituents in **PS1-PS4**. This is due to the more electron-deficient nitrogen atom in the ammonium salt. Fig. 3 and Fig. S20 show the comparative ^{1}H NMR spectra of **PS1** and **PS1a** in DMSO-d_6, while Fig. S23 shows those of **PS2** and **PS2a**. Both figures serve as illustrative examples. Fig. 3 shows that the $(CH_3)_3N^+$– protons of **PS1a** appear considerably deshielded by 0.93

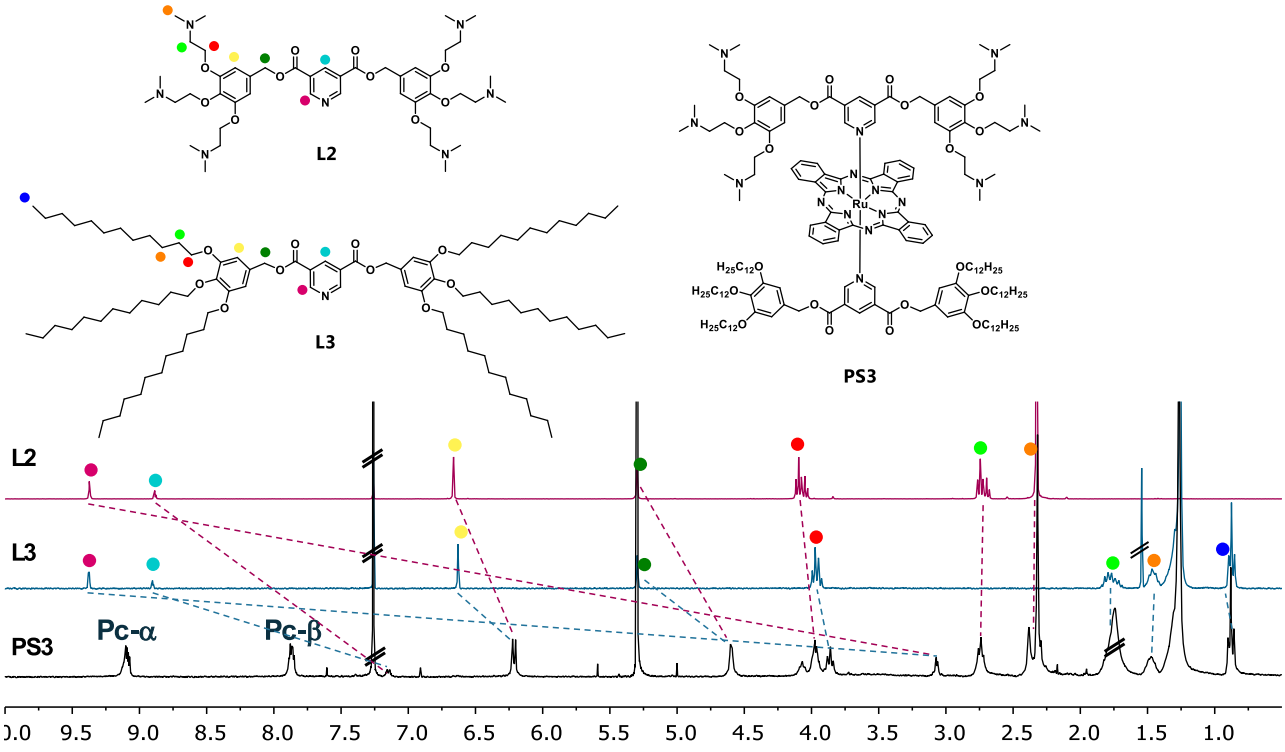

Fig. 2. Comparative ^{1}H NMR spectra of **L2**, **L3** and **PS3** in $CDCl_3$.

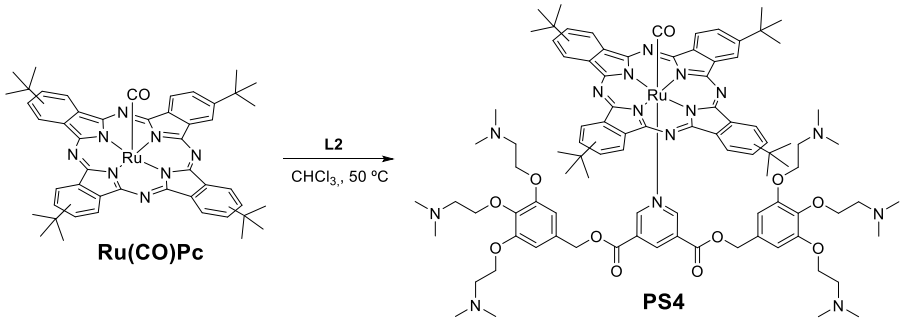

Scheme 3. Preparation of **PS4**.

ppm compared to the corresponding amino substituents in **PS1**. The effect is even stronger for the ammonium methylene protons $–N^{+}CH_2–$, which are down-field shifted by 1.45 ppm. The same behaviour is observed for **PS2a**, as shown in Fig. S23. Here, the $(CH_3)_3N^{+}–$ protons undergo a down-field shift of 1.02 ppm, while the $–N^{+}CH_2–$ protons experience a down-field shift of 1.26 ppm. Additionally, the $–OCH_2–$ protons are shifted by 0.37 ppm compared to **PS2**.

The ^{1}H NMR spectrum of **PS3a** is shown in Fig. S26. The proton shifts of **L2** upon quaternization are similar to those observed for **PS2a**. Besides, the signal at 7.06 ppm corresponds to the H-4 pyridine proton. The singlets observed at 6.61 and 4.69 ppm correspond to the H-2′,6′ benzene and benzylic protons respectively. The $(CH_3)_3N^{+}–$ protons are observed as singlets at 3.19 ppm. Finally, the H-2,6-pyridine protons appear at 3.08 ppm. **PS4a** showed in ^{1}H NMR similar features for the proton signals of **L2** as those observed previously for **PS2a** and **PS3a**. In particular, methyl groups corresponding to $(CH_3)_3N^{+}–$ appear at 3.21 ppm, while the $–N^{+}CH_2-$ and $–OCH_2–$ moieties display signals at 3.82 and 4.28 ppm, respectively (Fig. S29).

2.2. UV–Vis spectra of PSs, aggregation and solubility studies

The UV–Vis absorption spectra of **PS1a**, **PS2a**, **PS3a** and **PS4a** recorded in DMSO are represented in Fig. S31. Table 2 includes the values of Q-band absorption maxima and absorption coefficients (ε).

As usually for bispyridyl RuPcs, the Q-band appeared as maxima at 628 nm for **PS1a-PS3a**, with extinction coefficients ranging from ca. 40000 to 70000 [46,51,52,55,56], and at 651 nm for **PS4a**, with higher extinction coefficient of 320000, as it corresponds to **Ru(CO)Pc** complexes [48,49]. None of the UV–Vis spectra indicate any influence of the hexacationic pyridyl ligand when compared to the **Ru(PhCN)$_2$Pc** or **Ru(CO)Pc** precursors, respectively.

The solubilities and aggregation properties of **PS1a**, **PS2a**, **PS3a**, and **PS4a** in various DMSO/PBS mixtures were evaluated using UV–Vis spectroscopy (Fig. 4). For each compound, eight solutions were prepared, with a constant concentration of PS across all solutions, ranging from neat DMSO to neat PBS (saturated solution). The PSs **PS1a and PS2a**, which are tetracationic and dodecationic respectively, exhibited a slight decrease in absorption intensity as the PBS ratio of the solvent increased. This reduction in absorption was more pronounced in the case of **PS1a**, which may be due to its lower solubility in this medium as

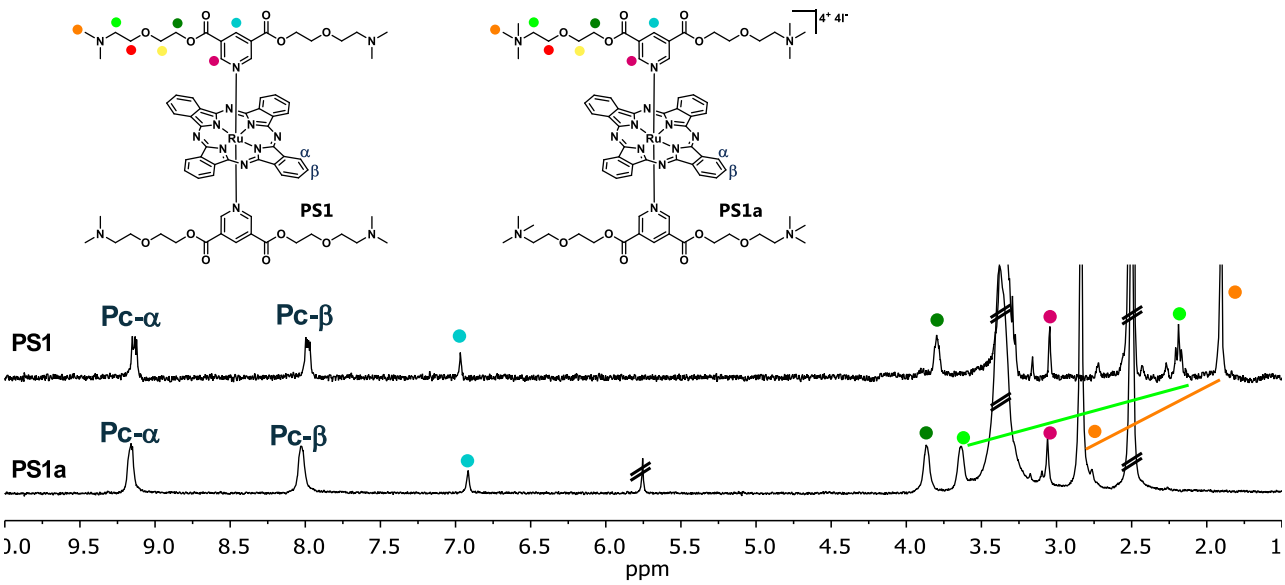

Fig. 3. Comparative ^{1}H NMR spectra of **PS1** and **PS1a** in DMSO-d_6.

Table 2
Q-band maxima and Φ_Δ in DMSO and n-octanol/PBS partition coefficients for **PS1a**, **PS2a**, **PS3a** and **PS4a**.

	λ_Q, nm (ε*10^{-4}, M^{-1}cm^{-1})	Φ_Δ	log $D_{7.4}$
PS1a	628 (6.74)	0.79	0.32
	628 (5.51)	0.65	0.09
PS2a			
	628 (4.32)	0.68	0.41
PS3a			
	651 (31.94)	0.52	1.08
PS4a			

it has eight fewer positive charges in its structure compared to **PS2a**. As both the Soret and Q-bands decreased by a similar order of magnitude, this effect is attributed to the partial precipitation of the PS as the water ratio increases, despite its considerable solubility in neat water. Actually, the difference between four positive charges in **PS1a** and twelve positive charges in **PS2a** is not significant. Although the relative ratio, as well as the position of B and Q-bands, is maintained upon addition of the PBS solution, there is a slight broadening of the Q-band in this experiment, therefore slight aggregation of **PS1a** and **PS2a** cannot be completely ruled out.

The amphiphilic nature of **PS3a** and **PS4a** makes the formation of micelles feasible owing to the hydrophobic effect. Hence, the tendency to aggregate in aqueous media is clearly evidenced through changes in their UV–Vis spectra upon increasing the percentage of PBS in the solvent. First, hexacationic **PS3a** exhibited a significant decrease in absorption intensity, indicating partial precipitation of the PS upon increasing the PBS ratio of the solvent. In addition, a progressive red shift of the Q-band maximum and broadening occurs at a PBS ratio of >25 %, suggesting the formation of aggregates. The effect is dramatic on going from 99.7 % PBS to neat PBS. Here, a sharp drop in PS absorbance, along with a marked broadening (189 nm half width compared to 157 nm in neat DMSO) and red shift of the Q-band maximum to 660 nm, is observed. For the hexacationic **PS4a**, aggregation is evidenced with lower percentages of PBS. There is a sudden drop in absorption from 5 % to 25 % of PBS, together with the appearance of a new band at around 700 nm, which intensity increases upon addition of PBS, at the same time as the Q-band intensity decreases and shifts up to 661 nm. The decrease in the Q/700 nm absorption ratio goes from $A_{657}/A_{700} = 6.2$ with 25 % PBS to $A_{661}/A_{700} = 1.3$ in neat PBS (Fig. 4).

2.3. Generation of singlet oxygen

Fig. S32 shows the degradation of DPBF ($\lambda_{max} = 417$ nm) when it is irradiated in the presence of **PS1a**, **PS2a**, **PS3a** and **PS4a**. The Φ_Δ values in DMSO for **PS1a**, **PS2a**, **PS3a** and **PS4a** are described on Table 2.

All evaluated photosensitizers demonstrated high quantum yields for singlet oxygen generation, ranging from 0.5 to 0.8, and consistent with the electron-deficient nature of the axial ligands in RuPcs [49,52,53]. The values of Φ_Δ are 0.7–0.8 for bispyridyl RuPcs **PS1a-PS3a**. **PS4a**, endowed with one pyridyl and one axial carbonyl ligands shows a slightly lower, though still good value of $\Phi_\Delta = 0.5$. This is in line with other previously described tetra-*tert*-butyl phthalocyanines with a carbonyl and a pyridyl axial ligands [57].

2.4. Determination of log $D_{7.4}$

The *n*-octanol/PBS partition coefficients of **PS1a**, **PS2a**, **PS3a** and **PS4a** (Table 2) were determined using the shake flask method as a preliminary evaluation of the relative lipophilicity of the PSs [58]. The log $D_{7.4}$ values of **PS1a**, **PS2a**, and **PS4a** compounds range from 0 to 1, indicating a favourable balance between permeability and solubility [58]. The relative order of lipophilicity is **PS4a** > **PS3a** > **PS1a** > **PS2a**. The dodecacationic nature of **PS2a** brings about the higher hydrophilicity observed for this compound. Between **PS1a** and **PS3a** displaying similar octanol/water partition coefficients, **PS3a**, with a higher number of ammonium rests results to be more lipophilic, as an effect of the six hydrocarbon chains at one of the axial ligands counteracting the six cationic charges at the other one. Between the two amphiphilic **PS3a** and **PS4a** containing six ammonium salts, the latter has a log $D_{7.4}$ value of 1.08, indicating greater hydrophobicity, despite the lower number of hydrocarbon chains (four compared to six in **PS3a**) and the lower number of carbon atoms for each (four compared to twelve in **PS3a**). The log $D_{7.4}$ values obtained for **PS1a-PS4a**, point to an influence, not only of their molecular structure, but also of their different tendencies to aggregate in PBS-containing media [59,60].

2.5. Photodynamic inactivation studies

The bispyridyl ruthenium phthalocyanines, **PS1a**, **PS2a**, and **PS3a** exhibited very high activity against antibiotic-resistant microorganisms (Fig. 5). All compounds showed higher activity against Gram-positive MRSA. This result aligns with the general trend for PDI, supported by

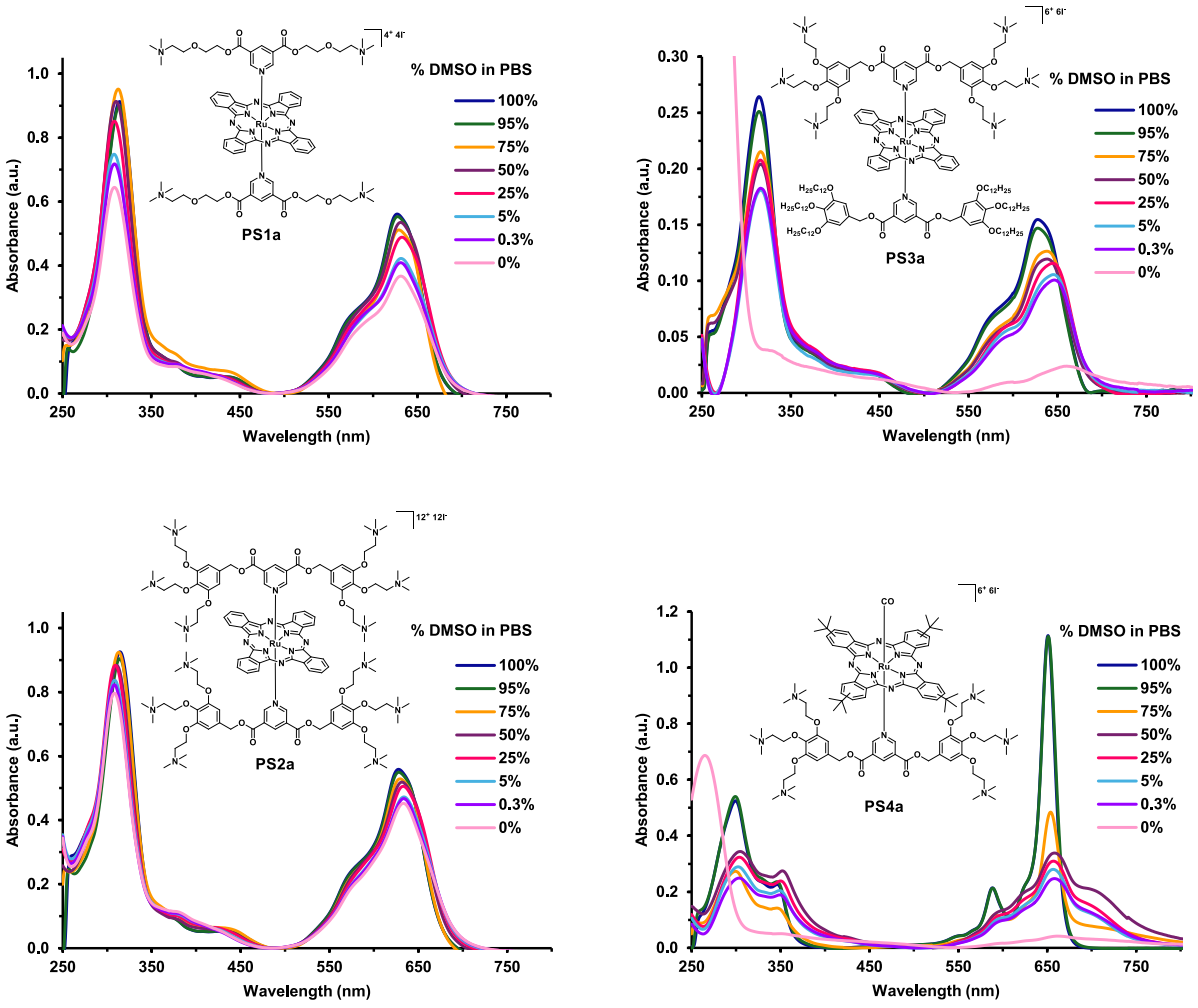

Fig. 4. UV–Vis solubility studies of **PS1a**, **PS2a**, **PS3a** and **PS4a** in different mixtures of DMSO/PBS.

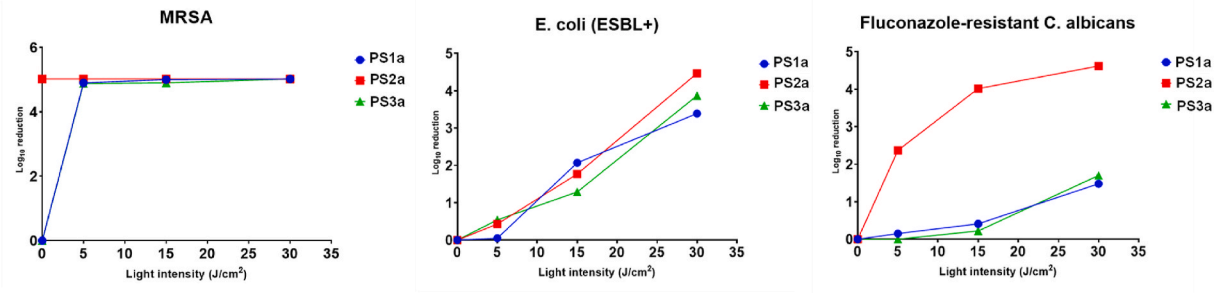

Fig. 5. The antibacterial activity of **PS1a-PS3a** under light irradiation against bacteria and fungi.

numerous scientific reports. Interestingly, **PS2a** showed very pronounced and strong dark toxicity, observed exclusively in Gram-positive bacteria. This phenomenon may be potentially related to the high molecular charge of the compound. It is likely that it exhibits activity similar to that observed with cationic disinfectants [61,62]. This is largely due to the absence of an outer lipid membrane in these bacteria, making them more susceptible to surfactants. In the case of **PS1a** and **PS3a**, their activity against MRSA is very high (about 5 log reduction). It is also noteworthy that even a very small dose of energy was sufficient to trigger a bactericidal response. This is a much stronger response than observed with zinc(II), palladium(II), and metal-free phthalocyanines, where a 5 log reduction effect against the same strain was only observed with light at a light dose of 100 J/cm^2 [63]. The same strain also proved to be much more resistant to non-peripheral octasubstituted zinc(II) phthalocyanines (150 J/cm^2, about 4 log reduction) [64]. Interestingly, tetra- and octasubstituted methimazole-phthalocyanine conjugates were completely inactive. This indicates that the direct expansion of substituents on the phthalocyanine ring itself may not be an optimal strategy for PDI [65]. Undoubtedly, the type of central atom also plays a key role, potentially related to the heavy metal effect, which may be

beneficial from the perspective of photodynamic therapy. In the case of Gram-negative bacteria, very high activity was also achieved, although the relationship between the structure and the effectiveness of PDI was much more pronounced. The compound **PS2a** acted most strongly and it is important to note that it did not induce dark toxicity in this case. Additional interaction studies indicated that **PS1a** systematically showed higher ability to cross cytoplasmic membrane for the three resistant microorganisms, despite its lower lipophilicity related to the amphiphilic **PS3a** (see Fig. 6 and Table 2). The lower uptake of **PS3a** respect to **PS1a** could be related to the higher tendency of the former to form aggregates. Besides, **PS2a** and **PS3a** exhibited the strongest interaction with the bacterial membrane/wall (Fig. 6). The combination of photodynamic properties with a possible impact on the physiological functioning of the bacterial wall/membrane system could have resulted in the highest antibacterial effect in the case of *E. coli* (ESBL+), where the activity reached approximately 4.5 log reduction for **PS2a**. At the same time, PDI targeting *E. coli* was associated with a much clearer time-effect relationship. This indicates a favourable balance between the efficiency of reactive oxygen species generation and the stability of the tested compounds under irradiation. In this case, the activity of compounds **PS1a**, **PS2a**, and **PS3a** at a concentration of 10^{-5} mol/dm^3 was incomparably higher than in the previous examples with other Pc complexes [63]. Interestingly, this trend was not observed for fungi. In fact, the results achieved by **PS1a** and **PS3a** cannot be classified as fungicidal (below 3 log reduction in growth), while lately reported zinc (II), palladium(II), and metal-free phthalocyanines exhibited activity between 4 and 5 log reduction, depending on the concentration and light dose used [63].

Completely different results were obtained for the compound **PS4a**, which also showed a significant difference in spatial structure compared to the other phthalocyanines, while having structural similarities to the most active compound tested, **PS2a**. **PS4a** did not exhibit activity against any of the tested strains (results significantly below the medically significant 3 log reduction threshold), whereas **PS1a**, **PS2a**, and **PS3a** did [66]. According to the calculated log$D_{7.4}$ values (Table 2) compound **PS4a** should achieve internal cell organelles. Therefore, the evaluation of the activity for **PS4a** was expanded to include additional pathogens showing antibacterial resistance, namely, methicillin-resistant *Staphylococcus epidermidis* (MRSE), *P. aeruginosa* (KPC+), and *K. pneumoniae* (MBL+) and (ESBL+) (Fig. 7). Interaction of **PS4a** with microbe membrane confirmed high ability to reach the interior of the cell (Fig. 7, right). It was observed that over 50 % of applicated PS dose was up taken into the cell (Fig. 7, right). This phenomenon did not impact on the activity against microbes. Only slight activity was noted for Gram-positive bacteria (ca. 2 log reduction) in contrast to Gram-negative and fungi (ca. 1 log reduction). However, this result remained without any potential clinical significance. Since **PS4a** showed high ability to achieve the interior of the cell, we decided to evaluate its combination with a classic antibiotic. Doxycycline was chosen because of its broad activity against both Gram-positive and Gram-negative bacteria. This antibiotic is a protein synthesis inhibitor that binds ribosomes and is characterized by a dominant bacteriostatic effect. The combination of **PS4a** and doxycycline showed greater activity against MRSA than the sum of the activities of each factor separately (see Fig. 8).

Sublethal PDI activity was used to evaluate the potential synergy effect of **PS4a** with the selected antibiotic. For *MRSA*, the positive potentially synergistic effect is most noticeable at the light dose of 30 J/cm^2 and a subinhibitory dose of the antibiotic (0.125 mg/L). However, such an effect was not observed for *E. coli* (ESBL+).

3. Conclusions

The effectivity of four hydrophilic ruthenium(II) phthalocyanines **PS1a-PS4a** as photosensitizers in PDI of multiresistant microorganisms was evaluated. These multicationic RuPcs bear from 4 to 12 terminal ammonium salts, attached to axial pyridyl substituents that strongly coordinate the Ru(II)Pc central ion. **PS1a-PS4a** were designed, on one side, to exhibit high singlet oxygen quantum yields, by donating them with electronically deficient, axial pyridyl ligands, and on the other side, to primarily target the microorganisms cytoplasmic cell membrane. In addition, **PS3a** and **PS4a** were endowed with amphiphilic character, for them to gradually diffuse into the inner cellular regions and exhibit multi-target localization. The two structurally different amphiphilic structures were assembled using different approaches, namely, by combining hexacationic and lipophilic axial substitution in a peripherally unsubstituted RuPc (**PS3a**), or by donating the peripheral positions of the RuPc scaffold with lipophilic substituents, while the axial sites bear a hexacationic and a carbonyl ligand, respectively (**PS4a**).

The hydrophilic **PS1a** and **PS2a**, as well as the amphiphilic **PS3a** show much stronger response against Gram-positive *MRSA* than that observed with zinc(II), palladium(II), and metal-free Pcs, which display similar efficiencies only using much higher light regimes. Likewise, the three PSs show exceptionally high activity against the Gram-negative *E. coli* at a concentration of 10^{-5} mol/dm^3. Conversely, fungicidal character against fluconazole-resistant *C. albicans* is only observed for **PS2a**.

Between **PS3a** and **PS4a**, the latter resulted to be more lipophilic. In fact, lipophilicity of **PS3a** is only slightly superior to that of **PS1a**, although this is not translated into higher cytoplasmic internalization for the former, which incorporation could also be influenced by the observed formation of aggregated species. On the other hand, despite over 50 % of the **PS4a** dose reached internal organelles, only slight photodynamic activity was noted for Gram-positive bacteria. However, **PS4a** shows a positive potentially synergistic effect against *MRSA* when combined with doxycycline. In particular, **PS4a**'s photodynamic activity increases from about 1.5 to about 4.9 log reduction under the light dose of 30 J/cm^2 and the 0.125 mg/L subinhibitory dose of the antibiotic.

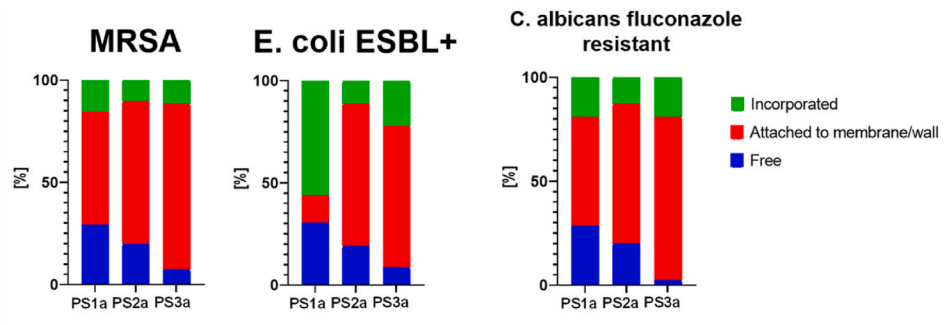

Fig. 6. Interaction PS-membrane for **PS1a-3a**.

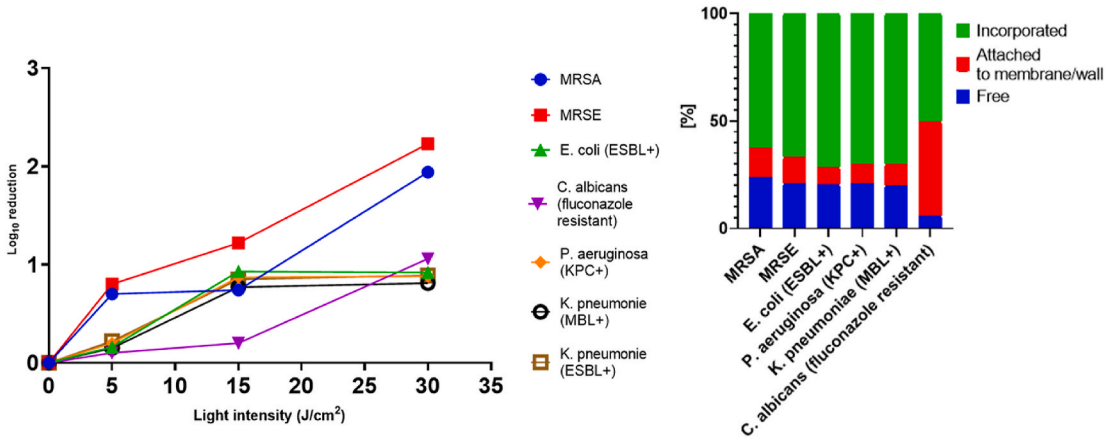

Fig. 7. Left – the inhibition rates of microbes growth for **PS4a**; right – interaction **PS4a**-membrane for evaluated microbes.

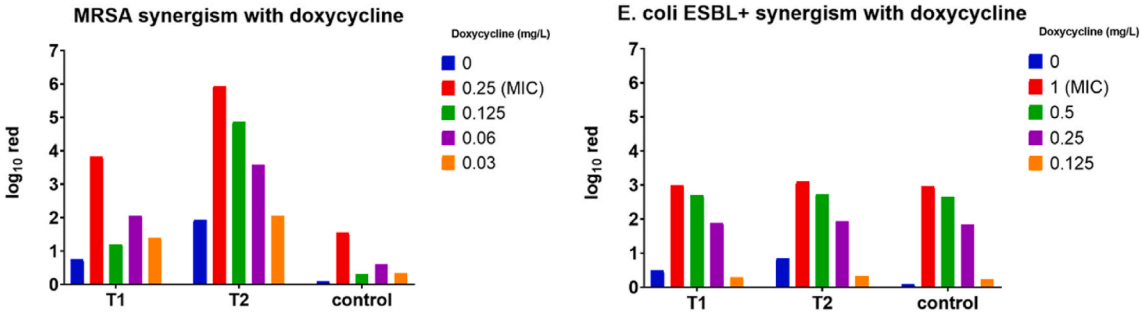

Fig. 8. The activity of **PS4a** in the presence of doxycycline under light irradiation (T1 = 5 J/cm^2 and T2 = 30 J/cm^2). MIC = minimum inhibitory concentration.

4. Experimental section

4.1. General information

4.1.1. Synthesis and instrumental analyses

Purification and separation of the synthesized products were performed by normal-phase column chromatography, using silica-gel (230–400 mesh, 0.040–0.063 mm, Merck) or aluminium oxide 90 active neutral (activity stage I, 70–230 mesh, 0.063–0.200 mm, Merck) and Biobeads SX-3. TLC was performed on aluminium sheets pre-coated with silica gel 60 F254 (E. Merck). Chemicals were purchased from commercial suppliers and used without further purification. "Synthetic grade" solvents were used for chemical reactions, column chromatography purifications, and "anhydrous grade" for reactions under dry conditions. The RuPc precursors **Ru(PhCN)$_2$Pc** [51] and **Ru(CO)Pc** [50] were prepared following reported procedures.

Nuclear magnetic resonance spectra (^{1}H, ^{13}C NMR) were recorded on a Bruker AV-300, or Bruker DRX-500 spectrometers, using as deuterated solvent, $CDCl_3$ or DMSO-d_6. All the experiments were recorded at room temperature. Chemical shifts are measured in ppm relative to tetramethylsilane (TMS). UV–Vis absortion spectra were recorded using solvents in the spectroscopic grade employing a JASCO V-660-Spectrophotometer. Infrared Spectra were recorded in solid state on a Bruker Alpha-II spectrophotometer by attenuated total reflection (ATR). High-resolution mass spectra (HRMS) were recorded employing matrix-assisted laser desorption/ionization time-of-flight (MALDI-TOF) using a Bruker-Ultraflex-III spectrometer with a Nd:YAG laser operating at 355 nm, or ultrafleXtreme spectrometer, or ESI-TOF using a Bruker Daltonics microTOF focus instrument.

4.1.2. Singlet oxygen quantum yields

The values of Φ_Δ were determined in DMSO using a reported methodology [67–69]. The photoinduced decomposition of 1,3-diphenylisobenzofuran (DPBF), which is an efficient $^1O_2$ quencher in organic media, was monitored through UV–Vis spectroscopy after irradiation with a halogen lamp of oxygen-saturated solutions of each PS and DPBF. Non-substituted ZnPc was used as the reference compound ($\Phi_\Delta = 0.67$ in DMSO).

Singlet oxygen quantum yields (Φ_Δ) were calculated using the following equation:

$$\phi_\Delta^S = \phi_\Delta^R \frac{k^S I_{aT}^R}{k^R I_{aT}^S}$$

Where k is the slope of a plot of $\ln(A_0/A_t)$ versus irradiation time t, with A_0 and A_t being the absorbance of the scavenger at the monitored wavelength (417 nm for DPBF) before and after irradiation time t, respectively. The superscripts R and S indicate reference and sample, respectively. I_{aT} is the total amount of light absorbed by the dye, calculated as the sum of intensities of the absorbed light I_a at wavelengths ranging from 530 nm (DMSO) to 800 nm (step 0.5 nm). A filter is used to completely filter off light under 530 nm, while the dye does not absorb light above 800 nm. I_a at a given wavelength is calculated using Beer's law:

$$I_a = I_0\left(1 - e^{-2.3A}\right)$$

Where I_0 corresponds to the transmittance of the filter at a given wavelength and A refers to the absorbance of the dye at that wavelength.

4.1.3. Determination of log $D_{7.4}$

The *n*-octanol/PBS partition coefficients were determined using the shake flask method as a preliminary evaluation of the relative lipophilicity of the PSs [58]. First, a water-saturated *n*-octanol solution of the compound was mixed with PBS (saturated with *n*-octanol) in a flask.

Subsequently, the flask was shaken to equilibrate the sample between the two phases. Finally, the concentration of PS in both phases was measured. To reduce analysis time, and prevent any errors arising from the different aggregation tendencies of the PSs in PBS (see Fig. 4) only the *n*-octanol phase will be analyzed, where no aggregation is detected (see Fig. S33). The concentration in the PBS phase will be obtained by difference. If the volumes of both phases are equal, the concentration of the compounds can be directly measured through their absorbance:

$$\log D_{7.4} = \log\left(\frac{c_{octanol}}{c_{PBS}}\right) = \log\left(\frac{A_{octanol}}{A_{PBS}} \times \frac{V_{PBS}}{V_{Octanol}}\right) = \log\left(\frac{A_{oct.final}}{A_{oct.inicial} - A_{oct.final}}\right)$$

4.2. Synthetic procedures and characterization

4.2.1. Synthesis of pyridyl-based ligands

*4.2.1.1. Bis(2,5-dioxopyrrolidin-*1-yl*) pyridine-3,5-dicarboxylate (1)* [54]. Trifluoroacetic anhydride (1.67 mL, 11.98 mmol) was added dropwise to a suspension of 3,5-pyridinedicarboxylic acid (1.00 g, 5.99 mmol), *N*-hydroxysuccinimide (NHS) (1.37 g, 13.17 mmol), and pyridine (1.94 mL, 23.96 mmol) in 7.5 mL of anhydrous chlorobenzene at 0 °C, under argon atmosphere. The resulting mixture was stirred at 0 °C for 15 min, and more chlorobenzene was added to reduce the viscosity of the mixture. Subsequently, stirring continued for 16 h at room temperature. The precipitate was isolated through filtration and washed with ethanol several times. After recrystallization from acetonitrile, 1.20 g of **1** (56 %) was obtained as a white solid. ^{1}H NMR (300 MHz, DMSO-d_6) δ(ppm): 9.58 (d, J = 2.1 Hz, 2H, py-H^{2,6}), 8.88 (t, J = 2.1 Hz, 1H, py-H^4), 2.92 (s, 8H, H$^{3',4'}$).

4.2.1.2. Pyridine-3,5-dicarboxylic acid bis-(2-[2-(dimethylamine)-ethoxy]-ethyl) ester (L1) [51]. A mixture of 2-[2-(dimethylamino) ethoxy]ethanol (268 mg, 2.01 mmol) and **1** (291 mg, 0.80 mmol) in 8 mL of dry DMF was stirred overnight, under argon, at room temperature. After evaporation of the solvent, the crude was dissolved in $CHCl_3$ and washed with water. The organic phase was dried over $MgSO_4$ and concentrated under reduced pressure. The residue was purified by column chromatography on neutral aluminium oxide (activity grade I, according to Brockmann), using a mixture of $CHCl_3$/Heptane (2:1) as eluent, affording 108 mg of **L1** (34 %) as a yellow oil. ^{1}H NMR (300 MHz, $CDCl_3$) δ(ppm): 9.37 (d, J = 2.1 Hz, 2H, py-H^{2,6}), 8.87 (t, J = 2.1 Hz, 1H, py-H^4), 4.54 (t, J = 4.9 Hz, 4H, H$^{1'}$), 3.81 (t, J = 4.8 Hz, 4H, H$^{2'}$), 3.62 (t, J = 5.7 Hz, 4H, H$^{3'}$), 2.52 (t, J = 5.7 Hz, 4H, H$^{4'}$), 2.26 (s, 12H, NCH_3). ^{13}C NMR (75.5 MHz, $CDCl_3$) δ(ppm): 164.35, 154.27, 138.09, 125.97, 69.39, 68.71, 64.72, 58.72, 45.80. HRMS (HR-ESI-QTOF, ionizing phase: MeOH + 0.1 % formic acid): Calcd for [$C_{19}H_{31}N_3O_6$]: 398.2291 [M+H]$^+$, 199.6185 [M+2H]$^{2+}$; Found: 398.2278 [M+H]$^+$, 199.6172 [M+2H]$^{2+}$.

4.2.1.3. Methyl 3,4,5-tris(2-(dimethylamino)ethoxy)benzoate (2). Gallic acid methyl ester (3.00 g, 16.29 mmol), 2-dimethylaminoethyl chloride hydrochloride (10.60 g, 73.31 mmol) and Cs_2CO_3 (64.00 g, 195.48 mmol) were dissolved in acetone (80 mL) and the solution was refluxed under argon for 72 h. The mixture was poured into 200 mL of water, transferred to a separatory funnel and extracted with chloroform. The organic phase was dried over anhydrous $MgSO_4$, filtered and the solvent was evaporated under reduced pressure. The crude was purified by column chromatography on silica gel using a mixture of AcOEt/MeOH/TEA (88:10:2) as the eluent. 5.81 g of compound **2** (90 %) was obtained as a brown oil. ^{1}H NMR (300 MHz, $CDCl_3$) δ(ppm): 7.29 (s, 2H, Ar-H^{2,6}), 4.2–4.1 (m, 6H, OCH_2), 3.89 (s, 3H, OCH_3), 2.8–2.7 (m, 6H, NCH_2), 2.43 (s, 6H, NCH_3), 2.35 (s, 12H, NCH_3).

4.2.1.4. (3,4,5-tris(2-(dimethylamino)ethoxy)phenyl)methanol (3). **2** (1.30 g, 3.38 mmol) was dissolved in dry THF (10 mL), and 13.6 mL of 1 M solution of $LiAlH_4$ in THF was added at 0 °C under argon. The reaction mixture was allowed to reach room temperature and stirred overnight. The resulting solution was poured into crushed ice, transferred to a separatory funnel, and extracted with $CHCl_3$. The organic phase was dried over anhydrous $MgSO_4$. After filtration of the desiccant, the solvent was evaporated under reduced pressure affording 950 mg (76 %) of **3** as a brown oil. ^{1}H NMR (300 MHz, $CDCl_3$) δ(ppm): 6.59 (s, 2H, Ar-H^{2,6}), 4.59 (s, 2H, C$\underline{H_2}$OH), 4.1–4.00 (m, 6H, OCH_2), 2.8–2.7 (m, NCH_2), 2.32 (s, 18H, NCH_3).

4.2.1.5. Bis(3,4,5-tris(2-(dimethylamino)ethoxy)benzyl) pyridine-3,5-dicarboxylate (L2). A mixture of **3** (950 mg, 2.57 mmol) and **1** (372 mg, 1.03 mmol) in 10 mL of dry DMF was stirred overnight at room temperature under argon. The solvent was evaporated under reduced pressure and the crude was dissolved in $CHCl_3$, transferred to a separatory funnel, and washed with water. The organic phase was dried over $MgSO_4$ and concentrated *in vacuo* after filtration. The residue was purified by column chromatography on neutral alumina (activity grade I, according to Brockmann), using $CHCl_3$/MeOH (100:1) as the eluent. 313 mg of **L2** (35 %) were obtained as a yellow oil. ^{1}H NMR (300 MHz, $CDCl_3$) δ(ppm): 9.37 (d, J = 2.2 Hz, 2H, py-H^{2,6}), 8.89 (t, J = 2.2 Hz, 1H, py-H^4), 6.67 (s, 4H, Ar-H$^{2',6'}$), 5.30 (s, 4H, OC$\underline{H_2}$Ph), 4.1–4.0 (m, 12H, H$^{2'}$), 2.8–2.7 (m, 12H, H$^{3'}$), 2.33 (s, 36H, NCH_3). ^{13}C NMR (75.5 MHz, $CDCl_3$) δ(ppm): 164.3, 154.4, 153.0, 138.5, 130.67, 126.12, 107.8, 70.95, 67.3, 59.0, 58.3, 46.0. HRMS (HR-ESI-QTOF, ionizing phase: MeOH + 0.1 % formic acid): Calcd for [$C_{45}H_{71}N_7O_{10}$]: 870,5341 [M+H]$^+$, 435,7710 [M+2H]$^{2+}$, 290.8499 [M+3H]$^{3+}$; Found: 870.5309 [M+H]$^+$, 435.7693 [M+2H]$^{2+}$, 290.8482 [M+3H]$^{3+}$. FT-IR (ATR) ν(cm^{-1}): 2941, 2864, 2819, 2768, 1725, 1591, 1504, 1437, 1366, 1329, 1306, 1227, 1189, 1159, 1116, 1027, 957, 827, 785, 746.

4.2.1.6. Dodecyl 4-methylbenzenesulfonate (4). A mixture of 1-dodecanol (5.00 g, 26.83 mmol), 4-toluene sulfonyl chloride (6.10 g, 32 mmol), TEA (3.20 g, 32 mmol) and a catalytic amount of DMAP in 40 mL of DCM, was stirred overnight at room temperature. The solution was transferred to a separatory funnel, washed with diluted HCl (aq), then with 0.5 M $NaHCO_3$ (aq) and dried over anhydrous Mg_2SO_4. After filtration of the desiccant and evaporation of the solvent, the product was purified by column chromatography on silica gel using DCM/heptane (1:4) as the eluent, affording 7.10g of **4** (77 %) as a colourless oil. ^{1}H NMR (300 MHz, $CDCl_3$) δ(ppm): 7.79 (d, J = 7.8 Hz, 2H, Ar–H), 7.34 (d, J = 8.0 Hz, 2H, Ar–H), 4.02 (t, 2H, OCH_2), 2.45 (s, 3H, Ar-C$\underline{H_3}$), 1.7–1.6 (m, 2H, CH_2), 1.3–1.2 (m, 18H, CH_2), 0.9–0.9 (m, 3H, CH_3).

4.2.1.7. Methyl 3,4,5-tris(dodecyloxy)benzoate (5). Gallic acid methyl ester (639 mg, 3.47 mmol), **4** (5.30 g, 15.62 mmol) and K_2CO_3 (4.80 g, 35.02 mmol) were dissolved in acetone (20 mL) and stirred at 62 °C, under argon, for 2 days. The reaction mixture was poured into 100 mL of water and extracted with chloroform. The organic phase was dried over anhydrous $MgSO_4$, filtered and concentrated at reduced pressure. The crude was purified by column chromatography on silica gel using a 1:2 mixture of $CHCl_3$/heptane as the eluent, affording 1.63 g of **5** (68 %) yield as a white solid. ^{1}H NMR (300 MHz, $CDCl_3$) δ(ppm): 7.25 (s, 2H, Ar-H^{2,6}), 4.0–4.0 (m, 6H, OCH_2), 3.89 (s, 3H, CO_2CH_3), 1.9–1.7 (m, 6H, H$^{3'}$), 1.5–1.4 (m, 6H, H$^{4'}$), 1.26 (s, 48H, CH_2), 0.9–0.9 (m, 9H, CH_3).

4.2.1.8. (3,4,5-tris(dodecyloxy)phenyl)methanol (6). 3 mL of a 1 M solution of $LiAlH_4$ in THF was added at 0 °C under argon to a solution of **5** (545 mg, 0.79 mmol) in dry THF (5 mL). The reaction mixture was allowed to reach room temperature and stirred overnight. The resulting solution was poured into crushed ice, transferred to a separatory funnel, and extracted with DCM. The organic phase was dried over anhydrous $MgSO_4$, the desiccant was filtered and rotary evaporated affording 449 mg of **6** (86 %) as a white solid. ^{1}H NMR (300 MHz, $CDCl_3$) δ(ppm): 6.56 (s, 2H, Ar-H^{2,6}), 4.59 (d, J = 5.9 Hz, 2H, PhC$\underline{H_2}$OH), 4.0–3.9 (m, 6H, OCH_2), 1.8–1.7 (m, 6H, H$^{3'}$), 1.5–1.4 (m, 6H, H$^{4'}$), 1.26 (s, 48H, CH_2), 0.9–0.9 (m, 9H, CH_3).

4.2.1.9. Bis(3,4,5-tris(dodecyloxy)benzyl)pyridine-3,5-dicarboxylate (L3). To a solution of 3,5-pyridinedicarboxylic acid (46 mg, 0.28 mmol) and DIPEA (145 mg, 1.12 mmol) in 15 mL of dry DCM, at 0 °C, COMU (247 mg, 0.58 mmol) was added, and the mixture was stirred at room temperature, under argon, for 30 min. Then, **6** (400 mg, 0.61 mmol) was added, and the stirring continued overnight. The solution was transferred to a separatory funnel and washed with aqueous $NaHCO_3$, then with diluted HCl and finally with water. The organic

phase was dried over anhydrous $MgSO_4$, and after filtration, the solvent was rotary evaporated. The residue was purified by column chromatography on silica gel using chloroform/heptane (5:4) as the eluent, affording 150 mg of **L3** (37 %) as a white solid. ^{1}H NMR (300 MHz, $CDCl_3$) δ(ppm): 9.38 (d, $J = 2.1$ Hz, 2H, py-H^{2,6}), 8.90 (t, $J = 2.1$ Hz, 1H, py-H^4), 6.63 (s, 4H, Ar-H$^{2',6'}$), 5.30 (s, 4H, -OC$\underline{H}_2$Ph), 4.0–3.9 (m, 12H, H$^{2'}$), 1.8–1.6 (m, 12H, H$^{3'}$), 1.5–1.4 (m, 12H, H$^{4'}$), 1.26 (s, 96H, CH_2), 0.9–0.9 (m, 18H, CH_3). ^{13}C NMR (75.5 MHz, $CDCl_3$) δ(ppm): 164.5, 154.4, 153.5, 138.8, 138.5, 130.2, 126.3, 107.5, 73.6, 69.4, 68.1, 32.1, 29.9, 29.9, 29.9, 29.8, 29.6, 29.5, 29.5, 26.3, 22.8, 14.3. FT-IR (ATR) ν(cm^{-1}): 2920, 2851, 1728, 1592, 1467, 1439, 1335, 1309, 1232, 1119. HRMS (HR-MALDI-TOF/TOF, matrix DCTB + PEGNa 1500 + NaI): Calcd. for [$C_{93}H_{161}NO_{10}$]: 1475,2018 [M+Na]$^+$; Found: 1475.2047 [M+Na]$^+$.

4.2.2. Coordination reactions to *Ru(PhCN)$_2$Pc*

*4.2.2.1. General procedure for the synthesis of **PS1**, **PS2** and **PS3**.* **Ru(PhCN)$_2$Pc** and excess of the ligands were stirred in the solvent, under argon, and protected from light. The specific quantities of reactants, reaction temperatures, and solvents used for each reaction are specified below. The progress of the reaction was monitored using ^{1}H NMR in $CDCl_3$. Upon reaction completion, the solvent was evaporated under reduced pressure, and the residue was further treated as detailed below.

*4.2.2.1.1. **PS1**.* Prepared from **Ru(PhCN)$_2$Pc** (10.0 mg, 0.012 mmol) and **L1** (10.7 mg, 0.027 mmol) in toluene at 60 °C overnight. The crude was precipitated with hexane, affording 13.3 mg of **PS1** (79 %) as a blue solid. ^{1}H NMR (300 MHz, $CDCl_3$) δ(ppm): 9.21 (dd, $J = 5.6$, 3.0 Hz, 8H), 7.92 (dd, $J = 5.7$, 3.0 Hz, 8H), 7.20 (t, $J = 1.9$ Hz, 2H), 3.88 (t, $J = 5.3$ Hz, 8H), 3.5–3.4 (m, 16H), 3.12 (d, $J = 1.8$, 4H), 2.36 (t, $J = 5.7$ Hz, 8H), 2.16 (s, 24H). ^{13}C NMR (75.5 MHz, $CDCl_3$) δ(ppm): 160.9, 154.4, 143.9, 140.8, 135.0, 128.3, 125.3, 121.7, 69.3, 38.1, 64.3, 58.7, 45.8. FT-IR (ATR) ν(cm^{-1}): 2955, 2870, 1737, 1656, 1599, 1489, 1414, 1364, 1324, 1290, 1240, 1169, 1123, 1066, 1035, 779, 754, 738. HRMS (HR-ESI-QTOF, ionizing phase: MeOH + 0.1 % formic acid): Calcd for [$C_{70}H_{78}N_{14}O_{12}^{96}$Ru]: 1403.5072 [M+H]$^+$. Found: 1403.5069 [M+H]$^+$.

*4.2.2.1.2. **PS2**.* Prepared from **Ru(PhCN)$_2$Pc** (10.0 mg, 0.012 mmol) and **L2** (23.5 mg, 0.027 mmol) in toluene at 60 °C overnight. The crude was purified by size exclusion chromatography on Biobeads SX-3 using DCM as the eluent. The resulting fraction containing **PS2** was precipitated with hexane, affording 13.8 mg of **PS2** (49 %) as a blue solid. ^{1}H NMR (300 MHz, $CDCl_3$) δ(ppm): 9.09 (dd, $J = 5.6$, 3.0 Hz, 8H), 7.87 (dd, $J = 5.7$, 3.0 Hz, 8H), 7.14 (t, $J = 1.8$ Hz, 2H), 6.23 (s, 8H), 4.60 (s, 8H), 4.1–4.0 (m, 24H), 3.07 (d, $J = 1.8$, 4H), 2.8–2.7 (m, 24H), 2.34, 2.34 (2 s, 72H). ^{13}C NMR (75.5 MHz, $CDCl_3$) δ(ppm): 161.1, 154.5, 152.9, 143.9, 140.71, 129.7, 128.3, 125.2, 121.6, 108.2, 71.1, 67.8, 59.2, 58.4, 46.2, 46.0. FT-IR (ATR) ν(cm^{-1}): 3357, 3050, 2930, 2822, 2775, 1660, 1621, 1590, 1489, 1438, 1414, 1352, 1326, 1290, 1267, 1230, 1168, 1118, 1065, 1033, 954, 755, 737, 720, 697. HRMS (HR-ESI-QTOF, ionizing phase: MeOH + 0.1 % formic acid): Calcd for [$C_{122}H_{158}N_{22}O_{20}^{96}$Ru]: 2350.1211 [M+H]$^+$, 1186.0547 [M + H + Na]$^{2+}$; Found: 2350.1257 [M+H]$^+$, 1186.0579 [M + H + Na]$^{2+}$.

*4.2.2.1.3. **PS3**.* Prepared from **Ru(PhCN)$_2$Pc** (10.0 mg, 0.012 mmol), **L2** (11.5 mg, 0.013 mmol) and **L3** (19.2 mg, 0.013 mmol) in $CHCl_3$ at room temperature for 5 days. The crude was purified by size exclusion chromatography on Biobeads SX-3 using DCM as the eluent. The fraction containing **PS3** was washed with hexane to give 2.8 mg (8 %) as a blue solid. ^{1}H NMR (300 MHz, $CDCl_3$) δ(ppm): 9.1–9.0 (m, 8H), 7.9–7.8 (m, 8H), 7.16, 7.13 (2 t, 2H), 6.22, 6.20 (2 s, 8H), 4.60, 4.59 (2 s, 8H), 4.1–3.9 (m, 12H), 2.86 (t, 12H), 3.07, 3.06 (2 d, 4H), 2.74 (t, 12H), 2.38, 2.32 (2 s, 36H), 1.8–1.7 (m, 12H), 1.5–1.4 (m, 12H), 1.27 (s, 96H), 0.88 (t, 18H).

4.2.3. Coordination reactions to *Ru(CO)Pc A*

***PS4*.** **Ru(CO)Pc** (10.0 mg, 0.011 mmol) and **L2** (11.4 mg, 0.013 mmol) were stirred in $CHCl_3$ at 50 °C under argon and protected from light for 3 days. Upon reaction completion, the solvent was evaporated under reduced pressure, and the resulting residue was used in next step without any purification.

4.2.4. Quaternization of the amines

General procedure for the synthesis of PS1a, PS2a, PS3a and PS4a

MeI was added to a solution of **PS1-4** in dry DMF, respectively. The reaction mixture was stirred at room temperature, under argon, and protected from light for 3 h. The quantities of MeI used for each reaction are specified below. The resulting solutions were then poured into MeOH (50 mL) and allowed to stand for 1 h. All volatiles were then evaporated under reduced pressure and the residue was treated as detailed below.

*4.2.4.1. **PS1a**.* **PS1** (10.0 mg, 0.0071 mmol); MeI (10.1 mg, 0.070 mmol). The residue was precipitated with DCM followed by filtration to give 13.2 mg of **PS1a** in 94 % yield. ^{1}H NMR (300 MHz, DMSO-d_6) δ(ppm): 9.16 (dd, $J = 5.6$, 3.0 Hz, 8H), 8.02 (dd, $J = 5.6$, 2.9 Hz, 8H), 6.92 (t, $J = 1.8$ Hz, 2H), 3.9–3.9 (m, 8H), 3.6–3.6 (m, 8H), 3.4–3.3 (m, 16H), 3.07 (d, $J = 1.8$, 4H); 2.84 (s, 36H). ^{13}C NMR (75.5 MHz, $CDCl_3$) δ(ppm): 160.4, 153.0, 143.1, 139.9, 128.7, 125.0, 121.5, 67.3, 64.2, 64.0, 63.7, 52.9. HRMS (HR-ESI-QTOF, ionizing phase: MeOH + 0.1 % TFA): Calcd. for [$C_{74}H_{90}N_{14}O_{12}^{96}$Ru]: 365.6479, Found: 365.6477 [M-4TFA]$^{4+}$.

*4.2.4.2. **PS2a**.* **PS2** (10.0 mg, 0.0042 mmol); MeI (18.1 mg, 0.127 mmol). The residue was precipitated with DCM followed by filtration to give 8.2 mg of **PS2a** in 48 % yield. ^{1}H NMR (300 MHz, DMSO-d_6) δ(ppm): 9.07 (dd, $J = 5.6$, 3.0 Hz, 8H), 8.03 (dd, $J = 5.7$, 3.0 Hz, 8H), 7.02 (t, $J = 1.8$ Hz, 2H), 6.57 (s, 8H), 4.70 (s, 8H), 4.3–4.2 (m, 24H), 3.9–3.7 (m, 24H), 3.23, 3.17 (2 s, 108H), 3.06 (d, $J = 1.8$, 4H). FT-IR (ATR) ν(cm^{-1}): 3402, 3008, 2953, 1730, 1594, 1473, 1440, 1412, 1374, 1325, 1313, 1289, 1229, 1168, 1118, 1065, 1022, 950, 875, 754, 739. HRMS (HR-ESI-QTOF, ionizing phase: MeOH + 0.1 % TFA): Calcd. for [$C_{134}H_{194}N_{22}O_{20}^{102}$Ru][$CF_3COO$]$_{10}^{2+}$: 1832.1217; Found: 1832.1168 [M-2TFA]$^{2+}$.

*4.2.4.3. **PS3a**.* **PS3** (2.8 mg, 0.0010 mmol); MeI (2.0 mg, 0.014 mmol). The residue was purified by size exclusion chromatography on Biobeads using DCM as the eluent. The fraction containing **PS3a** was evaporated to give 0.9 mg of the final product in 25 % yield. ^{1}H NMR (300 MHz, DMSO-d_6) δ(ppm): 9.07–9.04 (dd, $J = 5.6$, 3.0 Hz, 8H), 7.99–7.96 (dd, $J = 5.8$, 3.0 Hz, 8H), 7.06, 6.99 (2 t, 2H), 6.61 (s, 4H), 6.15 (s, 4H), 4.70 (s, 4H), 4.58 (s, 4H), 4.3–4.3 (m, 12H), 3.9–3.7 (m, 12H), 3.6–3.5 (m, 12H), 3.25, 3.19 (2 s, 36H), 3.09, 3.03 (2 d, 4H), 1.8–1.7 (m, 12H), 1.5–1.4 (m, 12H), 1.18, 1.14, 1.10 (3 s, 96H), 0.81 (t, 18H). FT-IR (ATR) ν(cm^{-1}): 2923, 2853, 1733, 1592, 1489, 1467, 1440, 1414, 1377, 1326, 1309, 1289, 1234, 1168, 1121, 1066, 1007, 952, 754, 738. HRMS (HR-ESI-QTOF, ionizing phase: MeOH + 0.1 % TFA): Calcd. for [$C_{176}H_{266}N_{16}O_{20}^{96}$Ru][$CF_3COO$]$_4^{2+}$: 1736.4394; [$C_{176}H_{266}N_{16}O_{20}^{96}$Ru][$CF_3COO$]$_3^{3+}$: 1119.9644; Found: 1736.4398 [M-2TFA]$^{2+}$; Found: 1119.9660 [M-3TFA]$^{3+}$.

*4.2.4.4. **PS4a**.* **PS4** (crude reaction product); MeI (36.9 mg, 0.260 mmol). The residue was purified by size exclusion chromatography on Biobeads using DMF as the eluent. The fraction containing **PS4a** was evaporated to give 5.4 mg of the final product in 19 % yield related to **Ru(CO)Pc** (two steps). ^{1}H NMR (300 MHz, DMSO-d_6) δ(ppm): 9.3–9.2 (m, 8H), 8.3–8.2 (m, 4H), 7.15 (t, 1H), 6.76 (s, 4H), 4.50 (s, 4H), 4.3–4.3 (m, 4H), 3.9–3.7 (m, 4H), 3.21 (s, 38H), 1.74, 1.71 (2 s, 36H). HRMS (HR-ESI-QTOF, ionizing phase: MeOH + 0.1 % TFA): Calcd for [$C_{49}H_{48}N_8O^{96}$Ru]: 860.3021 [M−L2]$^+$, Found: 860.3015.

4.3. Antimicrobial activity

4.3.1. Microbial cultures

The following microbes were used in the experiment: methicillin-resistant *Staphylococcus aureus* (MRSA), *Staphylococcus epidermidis* (MRSE) (clinical strain), beta-lactamase-producing *Escherichia coli*

(clinical strain), *Candida albicans* fluconazole-resistant (clinical strain), *Pseudomonas aeruginosa* producing KPC-type enzymes, as well as beta-lactamase-producing *Klebsiella pneumoniae* and *Klebsiella pneumoniae* producing metallo-β-lactamases. Microorganisms were cultivated according to species-specific guidelines; in summary, all bacteria were cultured in brain heart infusion broth (bioMerieux, Marcy-l'Étoile, France) for approximately 20 h at a constant temperature of 35 ± 1 °C under aerobic conditions. *C. albicans* were cultivated for approximately 24 h at 35 ± 1 °C in Sabouraud dextrose broth (Oxoid, Hampshire, UK). After the incubation period, the bacteria and fungi were centrifuged and harvested (3000 rpm for 15 min) and then re-suspended in saline. In the final step, each strain was adjusted to a concentration of approximately 10^7 CFU/mL.

4.3.2. Dark activity

Dark activity tests were performed according to the previously described procedure. In summary, appropriately prepared suspensions of bacteria and fungi were exposed to PSs at a concentration of 10^{-5} mol/dm^3 for 30 min (pre-incubation). Then, a series of dilutions were prepared, and surface plating was performed on TSA (bacteria) and Sabouraud agar (fungi). The Petri dishes were incubated for 24 h at 35 ± 1 °C, and the number of colonies was counted. Additionally, a control test was conducted where the PS was replaced with a saline solution. By comparing the control and test samples, the log reduction was calculated. A reduction of more than 0.5 log was considered as a criterion for the occurrence of dark toxicity.

4.3.3. Light-dependent activity

Similarly to the dark activity, the light activity of the PS was evaluated. Bacteria and fungi were pre-incubated in a 96-well plate with PSs at a concentration of 10^{-5} mol/dm^3 for 30 min and then exposed to light of 660 nm wavelength at doses ranging from 5 to 30 J/cm^2. A control test was also performed where the PS solution was replaced with saline. After exposure, a series of dilutions were prepared, and surface plating was performed on TSA (bacteria) and Sabouraud agar (fungi). The plates were incubated for 24 h at 35 ± 1 °C, and the number of colonies was counted. The difference in bacterial counts between the non-irradiated control and the PS-containing sample was used to calculate the log reduction.

4.3.4. Determination of Microorganism's Susceptibility to PACT following habituation with MIC and sub-MIC doses of doxycycline

Bacterial suspensions of MRSA and *E. coli* (ESBL+) were prepared according to EUCAST guidelines [70] and subjected to doxycycline at concentrations corresponding to MIC, ½ MIC, ¼ MIC, and $^1/_8$ MIC. After 12 h, the bacterial concentration was adjusted to OD600 equal to 0.3, and then these bacterial suspensions were pre-incubated for 30 min with photosensitizer at a concentration of 10^{-5} mol/dm^3 in a 96-well plate. The mixture was then exposed to light of 660 nm wavelength and energies of 5 and 30 J/cm^2. Parallel tests without irradiation and without irradiation and PSs were also performed. The log reduction was calculated as in the previous section.

4.3.5. Determination of photosensitizer uptake by microorganism cells

Bacterial and fungal cultures were prepared according to point *4.3.2*. Then, 300 μL of PS solution at a concentration of 10^{-5} mol/dm^3 was added to the washed microorganisms and incubated for 30 min (conditions similar to those on the 96-well plate in point *4.3.3*. After this period, the bacteria were centrifuged (3000 RPM; 15 min) and collected, and the supernatant was aspirated and left for further studies (Solution 1). The microorganisms were then subjected to three cycles of shaking (1 min) and washing with saline, repeating centrifugation and supernatant aspiration each time. The washed bacteria were then disintegrated using the thermal method, subjecting the bacterial cell wall to lysis by warming up (60 ± 2 °C) and cooling down (−20 ± 2 °C) during six cycles lasting 30 s each [71]. Disintegrated bacteria were suspended in saline (Solution 2). The concentrations in Solutions 1 and 2 were measured spectrophotometrically, correcting for the appropriate dilution factors. Based on this, the percentage of internalized substance (Solution 2) and free substance (Solution 1) was determined. The percentage of bound substance was calculated as the difference between the total concentration (100 %) and the percentage content of the substance in Solution 2 and Solution.

CRediT authorship contribution statement

Ana Belén Domínguez: Writing – original draft, Methodology, Investigation. **Daniel Ziental:** Writing – original draft, Methodology, Investigation. **Jolanta Dlugaszewska:** Methodology, Investigation. **Lukasz Sobotta:** Writing – review & editing, Resources, Funding acquisition, Conceptualization. **Tomás Torres:** Resources, Funding acquisition, Conceptualization. **M. Salomé Rodríguez-Morgade:** Writing – review & editing, Writing – original draft, Supervision, Resources, Funding acquisition, Formal analysis, Conceptualization.

Declaration of competing interest

The authors have nothing to declare.

5. Acknowledgements

We acknowledge financial support from the Spanish Grant PID2020-116490GB-I00 funded by MCIN/AEI/10.13039/501100011033 and by the "European Union NextGenerationEU/PRTR, MCIU/AEI/10.13039/501100011033/FEDER, UE (PID2023-151167NB-I00), the Comunidad de Madrid and the Spanish State through the Recovery, Transformation and Resilience Plan ["Materiales Disruptivos Bidimensionales (2D)" (MAD2D-CM) (UAM1)-MRR Materiales Avanzados], and the European Union through the Next Generation EU funds. IMDEA Nanociencia acknowledges support from the "Severo Ochoa" Programme for Centres of Excellence in R&D (MINECO, Grant CEX2020-001039-S). A.B.D. acknowledges the Comunidad de Madrid and the European Union for a predoctoral research contract within the Youth Employment Operative Programme and the Youth Employment Initiative (YEI) (Contract PEJ-2019-AI/IND-14708).

Appendix. ASupplementary data

Supplementary data to this article can be found online at https://doi.org/10.1016/j.ejmech.2024.117214.

Data availability

Data will be made available on request.

References

[1] J. Murugaiyan, P. Anand Kumar, G.S. Rao, K. Iskandar, S. Hawser, J.P. Hays, Y. Mohsen, S. Adukkadukkam, W.A. Awuah, R.A.M. Jose, N. Sylvia, E. P. Nansubuga, B. Tilocca, P. Roncada, N. Roson-Calero, J. Moreno-Morales, R. Amin, B. Krishna Kumar, A. Kumar, A.R. Toufik, T.N. Zaw, O.O. Akinwotu, M. P. Satyaseela, M.B.M. van Dongen, Progress in alternative strategies to combat antimicrobial resistance: focus on antibiotics, Antibiotics 11 (2022) 200, https://doi.org/10.3390/ANTIBIOTICS11020200.

[2] B. Pucelik, J.M. Dąbrowski, Photodynamic inactivation (PDI) as a promising alternative to current pharmaceuticals for the treatment of resistant microorganisms, Adv. Inorg. Chem. 79 (2022) 65–108, https://doi.org/10.1016/BS.ADIOCH.2021.12.003.

[3] K. Plaetzer, B. Krammer, J. Berlanda, F. Berr, T. Kiesslich, Photophysics and photochemistry of photodynamic therapy: fundamental aspects, Laser Med. Sci. 24 (2009) 259–268, https://doi.org/10.1007/s10103-008-0539-1.

[4] C. Chen, H. Ou, R. Liu, D. Ding, C. Chen, H. Ou, R. Liu, D. Ding, Regulating the photophysical property of organic/polymer optical agents for promoted cancer phototheranostics, Adv. Mater. 32 (2020) 1806331, https://doi.org/10.1002/ADMA.201806331.

[5] C.S. Foote, DEFINITION of type I and type II photosensitized oxidation, Photochem. Photobiol. 54 (1991) 659, https://doi.org/10.1111/J.1751-1097.1991.TB02071.X, 659.

[6] T. Nyokong, Desired properties of new phthalocyanines for photodynamic therapy, Pure Appl. Chem. 83 (2011) 1763–1779, https://doi.org/10.1351/PAC-CON-10-11-22.

[7] C.M. Bergamini, S. Gambetti, A. Dondi, C. Cervellati, Oxygen, reactive oxygen species and tissue damage, Curr. Pharmaceut. Des. 10 (2005) 1611–1626, https://doi.org/10.2174/1381612043384664.

[8] M.R. Hamblin, H. Abrahamse, Oxygen-independent antimicrobial photoinactivation: type III photochemical mechanism? Antibiotics 9 (2020) 53, https://doi.org/10.3390/antibiotics9020053.

[9] M.A. Pereira, M.A.F. Faustino, J.P.C. Tomé, M.G.P.M.S. Neves, A.C. Tomé, J.A. S. Cavaleiro, Â. Cunha, A. Almeida, Influence of external bacterial structures on the efficiency of photodynamic inactivation by a cationic porphyrin, Photochem. Photobiol. Sci. 13 (2014) 680–690, https://doi.org/10.1039/C3PP50408E.

[10] A. Almeida, Photodynamic therapy in the inactivation of microorganisms, Antibiotics 9 (2020) 138, https://doi.org/10.3390/ANTIBIOTICS9040138.

[11] J.Y. Nagata, N. Hioka, E. Kimura, V.R. Batistela, R.S.S. Terada, A.X. Graciano, M. L. Baesso, M.F. Hayacibara, Antibacterial photodynamic therapy for dental caries: evaluation of the photosensitizers used and light source properties, Photodiagnosis Photodyn. Ther. 9 (2012) 122–131, https://doi.org/10.1016/J.PDPDT.2011.11.006.

[12] T. Dai, Y.Y. Huang, M.R. Hamblin, Photodynamic therapy for localized infections—state of the art, Photodiagn. Photodyn, Ther. 6 (2009) 170–188, https://doi.org/10.1016/J.PDPDT.2009.10.008.

[13] M.T. Wan, J.Y. Lin, Current evidence and applications of photodynamic therapy in dermatology, Clin. Cosmet. Invest. Dermatol. 7 (2014) 145–163, https://doi.org/10.2147/CCID.S35334.

[14] L. Huang, M. Wang, Y.Y. Huang, A. El-Hussein, L.M. Wolf, L.Y. Chiang, M. R. Hamblin, Progressive cationic functionalization of chlorin derivatives for antimicrobial photodynamic inactivation and related vancomycin conjugates, Photochem. Photobiol. Sci. 17 (2018) 638–651, https://doi.org/10.1039/c7pp00389g.

[15] C.P.S. Ribeiro, M.A.F. Faustino, A. Almeida, L.M.O. Lourenço, The antimicrobial photoinactivation effect on Escherichia coli through the action of inverted cationic porphyrin– cyclodextrin conjugates, Microorganisms 10 (2022) 718, https://doi.org/10.3390/microorganisms10040718.

[16] N.M.M. Moura, X. Moreira, E.S. Da Silva, J.L. Faria, M.G.P.M.S. Neves, A. Almeida, M.A.F. Faustino, A.T.P.C. Gomes, Efficient strategies to use β-cationic porphyrin-imidazolium derivatives in the photoinactivation of methicillin-resistant Staphylococcus aureus, Int. J. Mol. Sci. 24 (2023) 15970, https://doi.org/10.3390/ijms242115970.

[17] W. Xuan, L. Huang, Y. Wang, X. Hu, G. Szewczyk, Y.Y. Huang, A. El-Hussein, J. C. Bommer, M.L. Nelson, T. Sarna, M.R. Hamblin, Amphiphilic tetracationic porphyrins are exceptionally active antimicrobial photosensitizers: in vitro and in vivo studies with the free-base and Pd-chelate, J Biophotonics 12 (2019) e201800318, https://doi.org/10.1002/jbio.201800318.

[18] M.L. Agazzi, M.B. Ballatore, E. Reynoso, E.D. Quiroga, E.N. Durantini, Synthesis, spectroscopic properties and photodynamic activity of two cationic BODIPY derivatives with application in the photoinactivation of microorganisms, Eur. J. Med. Chem. 126 (2017) 110–121, https://doi.org/10.1016/j.ejmech.2016.10.001.

[19] T. Maisch, J. Baier, B. Franz, M. Maier, M. Landthaler, R.M. Szeimies, W. Bäumler, The role of singlet oxygen and oxygen concentration in photodynamic inactivation of bacteria, Proc. Natl. Acad. Sci. USA 104 (2007) 7223–7228, https://doi.org/10.1073/PNAS.0611328104.

[20] G. Jori, C. Fabris, M. Soncin, S. Ferro, O. Coppellotti, D. Dei, L. Fantetti, G. Chiti, G. Roncucci, Photodynamic therapy in the treatment of microbial infections: basic principles and perspective applications, Laser Surg. Med. 38 (2006) 468–481, https://doi.org/10.1002/LSM.20361.

[21] M. Klausen, M. Ucuncu, M. Bradley, Design of photosensitizing agents for targeted antimicrobial photodynamic therapy, Molecules 25 (2020) 5239, https://doi.org/10.3390/MOLECULES25225239.

[22] M.F.C. Silva, R.T. Aroso, J.M. Dabrowski, B. Pucelik, A. Barzowska, G.J. da Silva, L. G. Arnaut, M.M. Pereira, Photodynamic inactivation of *E. coli* with cationic imidazolyl-porphyrin photosensitizers and their synergic combination with antimicrobial cinnamaldehyde, Photochem. Photobiol. Sci. 23 (2024) 1129–1142, https://doi.org/10.1007/s43630-024-00581-y.

[23] R.R. Allison, G.H. Downie, R. Cuenca, X.H. Hu, C.J.H. Childs, C.H. Sibata, Photosensitizers in clinical PDT, photodiagn. Photodyn, Ther. 1 (2004) 27–42, https://doi.org/10.1016/S1572-1000(04)00007-9.

[24] J.H. Correia, J.A. Rodrigues, S. Pimenta, T. Dong, Z. Yang, Photodynamic therapy review: principles, photosensitizers, applications, and future directions, Pharmaceutics 13 (2021) 1332, https://doi.org/10.3390/PHARMACEUTICS13091332.

[25] I.S. Mfouo-Tynga, L.D. Dias, N.M. Inada, C. Kurachi, Features of third generation photosensitizers used in anticancer photodynamic therapy: review, Photodiagnosis Photodyn. Ther. 34 (2021) 102091, https://doi.org/10.1016/J.PDPDT.2020.102091.

[26] S.N. Nyamu, L. Ombaka, E. Masika, M. Ng'ang'a, Antimicrobial photodynamic activity of phthalocyanine derivatives, Adv. Chem. (2018) 2598062, https://doi.org/10.1155/2018/2598062.

[27] M.B. Spesia, E.N. Durantini, Evolution of phthalocyanine structures as photodynamic agents for bacteria inactivation, Chem. Rec. 22 (2022) e202100292, https://doi.org/10.1002/tcr.202100292.

[28] S. Zhou, N. Zheng, H. Li, K. Zheng, Phthalocyanine-based photosensitizers for photodynamic antibacterial therapy, ChemistrySelect 9 (2024) e202400451, https://doi.org/10.1002/slct.202400451.

[29] A.T.Y. Lau, Y. Wang, J.F. Chiu, Reactive oxygen species: current knowledge and applications in cancer research and therapeutic, J. Cell. Biochem. 104 (2008) 657–667, https://doi.org/10.1002/JCB.21655.

[30] N. Sekkat, H. Van Den Bergh, T. Nyokong, N. Lange, Like a bolt from the blue: phthalocyanines in biomedical optics, Molecules 17 (2011) 98–144, https://doi.org/10.3390/MOLECULES17010098.

[31] X. Li, J.F. Lovell, J. Yoon, X. Chen, Clinical development and potential of photothermal and photodynamic therapies for cancer, Nat. Rev. Clin. Oncol. 17 (2020) 657–674, https://doi.org/10.1038/s41571-020-0410-2.

[32] X. Li, D. Lee, J.-D. Huang, J. Yoon, Phthalocyanine-assembled nanodots as photosensitizers for highly efficient type I photoreactions in photodynamic therapy, Angew. Chem. Int. Ed. 57 (2018) 9885–9890, https://doi.org/10.1002/anie.201806551.

[33] K.L.M. Santos, R.M. Barros, D.P. da Silva Lima, A.M.A. Nunes, M.R. Sato, R. Faccio, B.P.G. de Lima Damasceno, J.A. Oshiro-Junior, Prospective application of phthalocyanines in the photodynamic therapy against microorganisms and tumor cells: a mini-review, Photodiagnosis Photodyn. Ther. 32 (2020) 102032, https://doi.org/10.1016/J.PDPDT.2020.102032.

[34] (a) T. Fukuda, N. Kobayashi, UV-Visible absorption spectroscopic properties of phthalocyanines and related macrocycles, in: K. Kadish, K. Smith, R. Guilard (Eds.), Handbook of Porphyrin Science, World Scientific Publishing Co., Singapore, 2010; (b) Y. Rio, M.S. Rodríguez-Morgade, T. Torres, Modulating the electronic properties of porphyrinoids: a voyage from the violet to the infrared regions of the electromagnetic spectrum, Org. Biomol. Chem. 6 (2008) 1877–1894, https://doi.org/10.1039/B800617B.

[35] P.C. Lo, M.S. Rodríguez-Morgade, R.K. Pandey, D.K.P. Ng, T. Torres, F. Dumoulin, The unique features and promises of phthalocyanines as advanced photosensitisers for photodynamic therapy of cancer, Chem. Soc. Rev. 49 (2020) 1041–1056, https://doi.org/10.1039/C9CS00129H.

[36] X. Li, B.-D. Zheng, X.-H. Peng, S.-Z. Li, J.-W. Ying, Y. Zhao, J.-D. Huang, J. Yoon, Phthalocyanines as medicinal photosensitizers: developments in the last five years, Coord. Chem. Rev. 379 (2019) 147–160, https://doi.org/10.1016/j.ccr.2017.08.003.

[37] M.S. Rodríguez-Morgade, T. Torres, Phthalocyanines and related compounds, in: Science of Synthesis Knowledge Updates, 2017, pp. 1–210.

[38] Y.I. Openda, B. Babu, T. Nyokong, Novel cationic-chalcone phthalocyanines for photodynamic therapy eradication of S. aureus and E. coli bacterial biofilms and MCF-7 breast cancer, Photodiagn. Photodyn, Ther. 38 (2022) 102863, https://doi.org/10.1016/J.PDPDT.2022.102863.

[39] D.D. Dominguez, A.W. Snow, J.S. Shirk, R.G.S. Pong, Polyethyleneoxide-capped phthalocyanines: limiting phthalocyanine aggregation to dimer formation, J. Porphyr. Phthalocyanines 5 (2001) 582–592, https://doi.org/10.1002/JPP.365.

[40] A.C. Yüzer, G. Kurtay, T. Ince, S. Yurtdaş, E. Harputlu, K. Ocakoglu, M. Güllü, C. Tozlu, M. Ince, Solution-processed small-molecule organic solar cells based on non-aggregated zinc phthalocyanine derivatives: a comparative experimental and theoretical study, Mater. Sci. Semicond. Process. 129 (2021) 105777, https://doi.org/10.1016/J.MSSP.2021.105777.

[41] Z. Biyiklioğlu, Water-soluble axially disubstituted non-aggregated silicon phthalocyanines and their electrochemical properties, Dyes Pigments 99 (2013) 59–66, https://doi.org/10.1016/J.DYEPIG.2013.04.017.

[42] Z. Wang, B. Shi, J. Zhu, Y. Xiong, X. Duan, X. Liao, J. Wang, Ruthenium terpyridine complexes based on dppz ligands as photodynamic antimicrobial agents against Staphylococcus aureus, New J. Chem. 48 (2024) 2806–2816, https://doi.org/10.1039/D3NJ04911F.

[43] R. Youf, A. Nasir, M. Müller, F. Thétiot, T. Haute, R. Ghanem, U. Jonas, H. Schönherr, G. Lemercier, T. Montier, T. Le Gall, Ruthenium(II) polypyridyl complexes for antimicrobial photodynamic therapy: prospects for application in cystic fibrosis lung airways, Pharmaceutics 14 (2022) 1664, https://doi.org/10.3390/PHARMACEUTICS14081664.

[44] C.P.S. Ribeiro, L.M.O. Lourenço, Overview of cationic phthalocyanines for effective photoinactivation of pathogenic microorganisms, J. Photochem. Photobiol., C 48 (2021) 100422, https://doi.org/10.1016/J.JPHOTOCHEMREV.2021.100422.

[45] A. Galstyan, Turning photons into drugs: phthalocyanine-based photosensitizers as efficient photoantimicrobials, Chem. Eur J. 27 (2021) 1903–1920, https://doi.org/10.1002/CHEM.202002703.

[46] T. Rawling, A. McDonagh, Ruthenium phthalocyanine and naphthalocyanine complexes: synthesis, properties and applications, Coord. Chem. Rev. 251 (2007) 1128–1157, https://doi.org/10.1016/J.CCR.2006.09.011.

[47] A.J. Jiménez, B. Grimm, V.L. Gunderson, M.T. Vagnini, S. Krick Calderon, M. S. Rodríguez-Morgade, M.R. Wasielewski, D.M. Guldi, T. Torres, Synthesis, characterization, and photoinduced energy and electron transfer in a supramolecular tetrakis (ruthenium(II) phthalocyanine) perylenediimide pentad, Chem. Eur J. 17 (2011) 5024–5032, https://doi.org/10.1002/CHEM.201002963.

[48] J. Fernández-Ariza, R.M. Krick Calderón, M.S. Rodríguez-Morgade, D.M. Guldi, T. Torres, Phthalocyanine-Perylenediimide cart wheels, J. Am. Chem. Soc. 138 (2016) 12963–12974, https://doi.org/10.1021/JACS.6B07432.

[49] J.T. Ferreira, J. Pina, C.A.F. Ribeiro, R. Fernandes, J.P.C. Tomé, M.S. Rodríguez-Morgade, T. Torres, Highly efficient singlet oxygen generators based on ruthenium phthalocyanines: synthesis, characterization and in vitro evaluation for photodynamic therapy, Chem. Eur J. 26 (2020) 1789–1799, https://doi.org/10.1002/CHEM.201903546.

[50] M.S. Rodríguez-Morgade, T. Torres, C. Atienza-Castellanos, D.M. Guldi, Supramolecular bis(rutheniumphthalocyanine)-perylenediimide ensembles: simple

complexation as a powerful tool toward long-lived radical ion pair states, J. Am. Chem. Soc. 128 (2006) 15145–15154, https://doi.org/10.1021/JA0622195.
[51] J.T. Ferreira, J. Pina, C.A.F. Ribeiro, R. Fernandes, J.P.C. Tomé, M.S. Rodríguez-Morgade, T. Torres, PEG-containing ruthenium phthalocyanines as photosensitizers for photodynamic therapy: synthesis, characterization and in vitro evaluation, J. Mater. Chem. B 5 (2017) 5862–5869, https://doi.org/10.1039/C7TB00958E.
[52] J.T. Ferreira, J. Pina, C.A.F. Ribeiro, R. Fernandes, J.P.C. Tomé, M.S. Rodríguez-Morgade, T. Torres, Synthesis, characterization and in vitro evaluation of carbohydrate-containing ruthenium phthalocyanines as third generation photosensitizers for photodynamic therapy, ChemPhotoChem 2 (2018) 640–654, https://doi.org/10.1002/CPTC.201800065.
[53] J.T. Ferreira, J. Pina, C.A.F. Ribeiro, R. Fernandes, J.P.C. Tomé, T. Torres, M. S. Rodríguez-Morgade, A ruthenium phthalocyanine functionalized with a folic acid unit as a photosensitizer for photodynamic therapy: synthesis, characterization and in vitro evaluation, J. Porphyr. Phthalocyanines 25 (2021) 1193–1202, https://doi.org/10.1142/S1088424621501224.
[54] T.M. Postma, W.R.J.D. Galloway, F.L. Cougnon, G.D. Pantoş, J.E. Stokes, D. F. Spring, Dynamic combinatorial chemistry with novel dithiol building blocks: towards new structurally diverse and adaptive screening collections, Synlett 24 (2013) 765–769. https://10.1055/s-0032-1318407.
[55] M.S. Rodríguez-Morgade, M. Planells, T. Torres, P. Ballester, E. Palomares, A colorimetric molecular probe for Cu(II) ions based on the redox properties of Ru (II) phthalocyanines, J. Mater. Chem. 18 (2007) 176–181, https://doi.org/10.1039/B712004D.
[56] M.S. Rodríguez-Morgade, M.E. Plonska-Brzezinska, A.J. Athans, E. Carbonell, G. De Miguel, D.M. Guldi, L. Echegoyen, T. Torres, Synthesis, characterization, and photoinduced electron transfer processes of orthogonal ruthenium phthalocyanine-fullerene assemblies, J. Am. Chem. Soc. 131 (2009) 10484–10496, https://doi.org/10.1021/JA902471W.
[57] L.E.S. Contreras, J. Zirzlmeier, S.V. Kirner, F. Setaro, F. Martínez, S. Lozada, P. Escobar, U. Hahn, D.M. Guldi, T. Torres, Cholesteryl oleate-appended phthalocyanines as potential photosensitizers in the treatment of leishmaniasis, J. Porphyr. Phthalocyanines 19 (2015) 320–328, https://doi.org/10.1142/S1088424615500157.
[58] A. Andrés, M. Rosés, C. Ràfols, E. Bosch, S. Espinosa, V. Segarra, J.M. Huerta, Setup and validation of shake-flask procedures for the determination of partition coefficients (log D) from low drug amounts, Eur. J. Pharmaceut. Sci. 76 (2015) 181–191, https://doi.org/10.1016/J.EJPS.2015.05.008.
[59] F.M. Engelmann, S.V.O. Rocha, H.E. Toma, K. Araki, M.S. Baptista, Determination of n-octanol/water partition and membrane binding of cationic porphyrins, Int. J. Pharm. 329 (2007) 12–18, https://doi.org/10.1016/j.ijpharm.2006.08.008.
[60] M. Ptak-Kaczor, M. Banach, K. Stapor, P. Fabian, L. Konieczny, I. Roterman, Solubility and aggregation of selected proteins interpreted on the basis of hydrophobicity distribution, Int. J. Mol. Sci. 22 (2021) 5002, https://doi.org/10.3390/ijms22095002.
[61] M. Vehapi, D. Özçimen, Antimicrobial and bacteriostatic activity of surfactants against B. subtilis for microbial cleaner formulation, Arch. Microbiol. 203 (2021) 3389–3397, https://doi.org/10.1007/s00203-021-02328-0.
[62] R. Najjar (Ed.), Application and Characterization of Surfactants, InTech, Jul. 05, 2017, https://doi.org/10.5772/65591.
[63] D. Ziental, D.T. Mlynarczyk, E. Kolasinski, E. Güzel, J. Dlugaszewska, Ł. Popenda, S. Jurga, T. Goslinski, L. Sobotta, Zinc(II), palladium(II), and metal-free phthalocyanines bearing nipagin-functionalized substituents against Candida auris and selected multidrug-resistant microbes, Pharmaceutics 14 (2022) 1686, https://doi.org/10.3390/pharmaceutics14081686.
[64] M. Wysocki, D. Ziental, Z. Biyiklioglu, M. Jozkowiak, H. Baş, J. Długaszewska, H. Piotrowska-Kempisty, E. Güzel, L. Sobotta, Non-peripheral octasubstituted zinc (ii) phthalocyanines bearing pyridinepropoxy substituents – antibacterial and anticancer photodynamic and sonodynamic activity, J. Inorg. Biochem. 262 (2024) 112751, https://doi.org/10.1016/j.jinorgbio.2024.112751.
[65] M. Wierzchowski, D. Ziental, D. Łazewski, A. Korzanski, A. Gielara-Korzanska, E. Tykarska, J. Dlugaszewska, L. Sobotta, New metallophthalocyanines bearing 2-methylimidazole moieties—potential photosensitizers against Staphylococcus aureus, Int. J. Mol. Sci. 23 (2022) 5910, https://doi.org/10.3390/ijms23115910.
[66] See, for example M. Ahrens, M. Spörer, H. Deppe, L.M. Ritschl, P. Mela, Bacterial reduction and temperature increase of titanium dental implant models treated with a 445 nm diode laser: an in vitro study, Sci. Rep. 14 (2024) 18053, https://doi.org/10.1038/s41598-024-68780-2.
[67] M.D. Maree, N. Kuznetsova, T. Nyokong, Silicon octaphenoxyphthalocyanines: photostability and singlet oxygen quantum yields, J. Photochem. Photobiol. Chem. 140 (2001) 117–125, https://doi.org/10.1016/S1010-6030(01)00409-9.
[68] J. Ma, J.Y. Chen, M. Idowu, T. Nyokong, Generation of singlet oxygen via the composites of water-soluble thiol-capped CdTe quantum dots-sulfonated aluminum phthalocyanines, J. Phys. Chem. B 112 (2008) 4465–4469, https://doi.org/10.1021/jp711537j.
[69] S. Makhseed, A. Tuhl, J. Samuel, P. Zimcik, N. Al-Awadi, V. Novakova, New highly soluble phenoxy-substituted phthalocyanine and azaphthalocyanine derivatives: synthesis, photochemical and photophysical studies and atypical aggregation behavior, Dyes Pigments 95 (2012) 351–357, https://doi.org/10.1016/j.dyepig.2012.03.023.
[70] D. Kamińska, M. Ratajczak, D.M. Nowak-Malczewska, J.A. Karolak, M. Kwaśniewski, A. Szumała-Kakol, J. Dlugaszewska, M. Gajecka, Macrolide and lincosamide resistance of *Streptococcus agalactiae* in pregnant women in Poland, Sci. Rep. 14 (2024) 3877, https://doi.org/10.1038/s41598-024-54521-y.
[71] D. Kaminska, M. Ratajczak, A. Szumała-Kąkol, J. Dlugaszewska, D.M. Nowak-Malczewska, M. Gajecka, Increasing resistance and changes in distribution of serotypes of *Streptococcus agalactiae* in Poland, Pathogen9 (2020) 526, https://doi.org/10.3390/pathogens9070526.